Coriolis effects in homogeneous and inhomogeneous katabatic flows

Alan Shapiro* and Evgeni Fedorovich
School of Meteorology, University of Oklahoma, Norman, Oklahoma, USA

ABSTRACT: Katabatic flows along a planar slope in a viscous stably-stratified fluid are investigated analytically and numerically, with an emphasis on flow features arising from the action of the Coriolis force. Two idealized flow types are considered: turbulent flow along a uniformly cooled slope, and two-dimensional laminar flow induced by a cold strip of finite width running down the slope. In the case of turbulent flow along a uniformly cooled slope, the downslope velocity exhibits a boundary-layer structure, but the cross-slope velocity and buoyancy fields spread inexorably upward. This behaviour is qualitatively similar to that found in laminar flows along a uniformly cooled slope. In contrast, in the two-dimensional strip flow, a steady state is reached, in which the cross-slope wind and buoyancy fields vanish far above the slope, but the downslope and slope-normal velocity fields do not vanish. These latter two flow components comprise two purely horizontal along-isentrope counter-flowing currents: an upslope current entering the top of the boundary layer on one side of the strip, and a downslope current flowing out of the boundary layer into the environment on the other side of the strip. The slope-normal vorticity associated with these currents originates in the stretching of planetary vorticity in a broad zone of convergent flow over the cold strip. Copyright © 2008 Royal Meteorological Society

1. Introduction

1.1. Katabatic and anabatic winds

Katabatic and anabatic winds are thermally driven air motions found in regions of complex terrain at all latitudes (Atkinson, 1981; Egger, 1990; Whiteman, 1990, 2000). When a sloping surface is cooled (katabatic flow case) or heated (anabatic flow case), a temperature difference is set up between the air in the surface layer and the environmental air at the same altitude. The buoyancy force associated with this temperature difference projects in the down- or up-slope direction and induces a down- or up-slope flow.

In areas that are largely sheltered from synoptic effects, katabatic and anabatic flows are the building blocks of local weather. Even in cases where synoptic forcing is important, pronounced katabatic and anabatic flow signatures may still exist. In regions where heavily industrialized population centres extend across variable topography, these local flows exert major controls over energy usage, visibility, fog formation and air pollutant dispersion (Lu and Turco, 1994; Fernando *et al*., 2001; Hunt *et al*., 2003; Lee *et al*., 2003; Brazel *et al*., 2005). In agricultural regions, these local winds significantly affect microclimates. On the larger scale, persistent katabatic winds cover vast areas of the earth (e.g. Antarctica,

Greenland), and play an important role in the weather and climate of these areas (Parish and Waight, 1987; Parish and Bromwich, 1991; Gallée and Schayes, 1994; Oerlemans, 1998; Renfrew, 2004; Renfrew and Anderson, 2006).

Katabatic and anabatic winds can be described in their most basic forms as turbulent natural convection flows along cooled/heated sloping surfaces in a stratified environment. Katabatic flows in particular are quite shallow (flow speed maximum is typically located 1–100 m above the slope), and are therefore poorly resolved in most numerical models. Although much progress has been made in the understanding and quantitative description of katabatic winds, long-standing difficulties with modelling stably-stratified turbulent flows along slopes, and the variety of flow interactions caused by complex topography and surface inhomogeneity, make the dynamics of these flows a rich and challenging area of study.

1.2. Motivation and scope of this investigation

An early milestone in the understanding of katabatic flows was Prandtl's (1942) one-dimensional (1D) model for the natural convection flow of a viscous stably-stratified fluid along a uniformly cooled sloping planar surface. Flow in the Prandtl model comprises a shallow downslope-flowing jet of cold air topped by a zone of weak warmer-than-ambient upslope flow. The model provides one of the few known exact analytical solutions of the Boussinesq equations of motion and

* Correspondence to: Alan Shapiro, Room 5900, School of Meteorology, University of Oklahoma, 120 David L. Boren Blvd., Norman, OK 73072, USA. E-mail: ashapiro@ou.edu

thermodynamic energy for a natural convection flow. It is conceptually simple and, when appropriately tuned, can provide qualitatively realistic descriptions of katabatic flows, especially at low levels (e.g. Defant, 1949; Tyson, 1968; Papadopoulos *et al.*, 1997; Oerlemans, 1998). The model has undergone several refinements within its 1D framework, including provision for nonlinear friction and heat exchange at the underlying surface (Ingel', 2000), vertically-varying eddy viscosities (Grisogono and Oerlemans, 2001, 2002), the Coriolis force (Gutman and Malbakhov, 1964), and the Coriolis force with external wind field (Lykosov and Gutman, 1972; Gutman and Melgarejo, 1981; Gutman, 1983). A curious feature of the 1D model when the Coriolis force is included is that the buoyancy and cross-slope momentum slowly but inexorably diffuse upward from the slope, eventually yielding steady-state solutions that do not have a boundary-layer character (Gutman and Malbakhov, 1964; Lykosov and Gutman, 1972; Egger, 1985). The behaviour of the cross-slope wind and buoyancy contrasts markedly with the downslope wind which retains a boundary-layer-type structure. Our present study on Coriolis effects in katabatic flows is motivated by this rather unusual and non-intuitive behaviour of the cross-slope wind and buoyancy fields.

Our study begins with a review of 1D katabatic flow theory with Coriolis effects (section 2), drawing attention to the unusual behaviour described above, and to other results which suggest that provision for an imposed external pressure-gradient force (or imposed geostrophic wind) cannot rectify the situation. Based on these results and related results on slope flows from the oceanographic literature, we suggest that the 1D Prandtl model with Coriolis force included is fundamentally inappropriate as a model of long-lived katabatic flows (at least of the buoyancy and cross-slope wind components), but can be made to be appropriate if additional processes are accounted for. Our view is that processes one might be inclined to discount from the outset as unimportant may, if persistent, be vital in controlling steady-state structure, especially of the cross-slope wind and buoyancy above the boundary layer. One such process may be a radiative thermal adjustment throughout the flow domain (Egger, 1985). Another process may be 2D or 3D effects associated with the finite extent of real katabatic flows (finite extent of slopes and/or surface forcings), which would break the 1D symmetry of the classical Prandtl framework.

In section 3 we conduct a preliminary analysis of the remote (far above slope) structure of the cross-slope wind and buoyancy in 2D and 3D frameworks. The slope is of infinite extent, but the surface forcing is restricted to be either periodic or of finite extent in the cross-slope and/or downslope directions. Because of these restrictions, our analysis should be applicable only to purely local katabatic flows, that is, to flows to which synoptic-scale forcings do not contribute.

In section 4 we present numerical simulation results for laminar and turbulent katabatic flows along a uniformly cooled surface with and without Coriolis effects. A key finding is that the inexorable upward growth of the cross-slope velocity and buoyancy fields that occur in laminar katabatic flow also occurs in explicitly simulated turbulent katabatic flow.

In section 5 we present a 2D linear analysis of laminar katabatic flow with Coriolis effects for the case where the surface forcing is of finite extent in the cross-slope direction (a strip of relatively cold surface running down the slope). The analysis shows that, in contrast to the 1D flow, the cross-slope wind and buoyancy fields in this 2D flow do vanish far above the slope. However, the downslope and slope-normal velocity components do not vanish far above the slope. Instead, these components comprise a purely horizontal (along-isentrope) streaming motion. Results from the analysis are confirmed and extended in section 6 with numerical simulations for the laminar flow regime. Conclusions follow in section 7.

1.3. Governing equations

Consider katabatic flow of a viscous stably-stratified fluid down a uniform planar slope inclined at angle α to the horizontal (Figure 1). The main object of our study is the steady-state structure of katabatic flows influenced by the Coriolis force. The analytical parts of our work are concerned exclusively with the steady state, while the numerical analyses are concerned with the steady state as the terminal state of an initial-value problem in which the atmosphere is initially at rest and an inhomogeneous surface buoyancy forcing is suddenly imposed.

Our work proceeds in a right-hand Cartesian (x, y, z) slope-following coordinate system with x axis pointing down the slope, y axis pointing across the slope along constant topographic height lines (into page on Figure 1), and z axis directed normal to the slope. The corresponding unit basis vectors are $\mathbf{i, j}$ and $\mathbf{k}$, respectively. The velocity vector $\mathbf{v} = u\mathbf{i} + v\mathbf{j} + w\mathbf{k}$ has down-, cross-slope and slope-normal components u, v and w, respectively. For future reference, note that the true vertical velocity component w^* ($\equiv \mathbf{k}^* \cdot \mathbf{v}$, where $\mathbf{k}^*$ is the unit vector pointing in the direction opposite the gravity vector) is related to the downslope and slope-normal velocity components by $w^* = u\mathbf{k}^* \cdot \mathbf{i} + w\mathbf{k}^* \cdot \mathbf{k} = -u\sin\alpha + w\cos\alpha$.

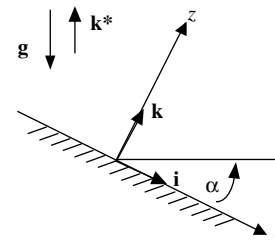In this slope-following coordinate system, the Boussinesq equations for katabatic flow on the rotating earth

Figure 1. Slope-following coordinate system: x is downslope coordinate, y is cross-slope coordinate (into page; not shown) and z is slope-normal coordinate.

are

$$\frac{\partial \theta'}{\partial t} + \mathbf{v} \cdot \nabla \theta' = \gamma (u \sin \alpha - w \cos \alpha) + \kappa \nabla^2 \theta', \quad (1.1)$$

$$\frac{\partial u}{\partial t} + \mathbf{v} \cdot \nabla u = -\frac{1}{\rho_r} \frac{\partial p'}{\partial x} + fv - g\frac{\theta'}{\theta_r}\sin\alpha + \nu\nabla^2 u,$$

$$(1.2)$$

$$\frac{\partial v}{\partial t} + \mathbf{v} \cdot \nabla v = -\frac{1}{\rho_r} \frac{\partial p'}{\partial y} - fu + \nu\nabla^2 v, \quad (1.3)$$

$$\frac{\partial w}{\partial t} + \mathbf{v} \cdot \nabla w = -\frac{1}{\rho_r} \frac{\partial p'}{\partial z} + g\frac{\theta'}{\theta_r}\cos\alpha + \nu\nabla^2 w, \quad (1.4)$$

$$\nabla \cdot \mathbf{v} = 0, \quad (1.5)$$

where (1.1) is the thermodynamic energy equation, (1.2) and (1.3) are the down- and cross-slope equations of motion, respectively, (1.4) is the slope-normal equation of motion, and (1.5) is the mass conservation equation for an incompressible fluid. Here $\theta' \equiv \theta - \theta_e$ is the perturbation potential temperature (θ is potential temperature, θ_e is the environmental potential temperature, a function only of the true vertical coordinate z^*), θ_r is a constant reference potential temperature, ρ_r is a constant reference density, g is the gravity acceleration, $\gamma \equiv \mathrm{d}\theta_e/\mathrm{d}z^*$ is the environmental temperature gradient, and $f \equiv 2\Omega \sin\phi$ is the Coriolis parameter (Ω is magnitude of the Earth's angular velocity vector $\boldsymbol{\Omega}$; ϕ is latitude). The parameters ν (viscosity) and κ (diffusivity) are treated as molecular coefficients in our three-dimensional turbulence simulations, and as effective eddy mixing coefficients in our two-dimensional laminar simulations. The parameters γ, f, ν and κ are considered constant. The perturbation pressure $p' \equiv p - p_e$ is the pressure p minus the hydrostatic pressure p_e based on the z^*-dependent environmental density profile. Since p_e is independent of the true horizontal coordinates, it cannot support a geostrophic flow. Accordingly, any geostrophic environmental flow we were to consider must be maintained by horizontal gradients of p'.

On the lower surface we impose the impermeability condition on the slope-normal velocity component, $w(x, y, 0, t) = 0$, and the no-slip condition on the down- and cross-slope velocity components, $u(x, y, 0, t) = 0$ and $v(x, y, 0, t) = 0$, respectively. The surface distribution of the perturbation potential temperature is specified (homogeneous or inhomogeneous, depending on the problem), and the slope-normal derivative of the perturbation pressure is calculated at the surface as a residual from (1.4). The slope-normal derivatives of all variables are considered to vanish far above the slope.

Equations (1.1)–(1.5) are similar to those considered in Shapiro and Fedorovich (2007), but with Coriolis terms included. Our treatment of the Coriolis terms is standard for models of katabatic winds along shallow slopes, that is, for slope angles on the order of a few degrees (e.g. Gutman and Malbakhov, 1964; Lykosov and Gutman, 1972; Gutman and Melgarejo, 1981; Mahrt, 1982; Egger, 1985). In (1.2) and (1.3), the down- and cross-slope components of the Coriolis force, $-\mathbf{i} \cdot (2\boldsymbol{\Omega} \times \mathbf{v})$ and $-\mathbf{j} \cdot (2\boldsymbol{\Omega} \times \mathbf{v})$, were approximated as fv and $-fu$, respectively. In arriving at those terms, the slope-normal component of the Earth's angular velocity, $\mathbf{k} \cdot \boldsymbol{\Omega}$, was replaced by the true vertical component of the Earth's angular velocity, $\mathbf{k}^* \cdot \boldsymbol{\Omega}$, a legitimate approximation for shallow slopes (error less than 0.4% for slope angles less than $5°$), and the contribution of the slope-normal velocity component w was neglected. In addition, the Coriolis force was neglected in the slope-normal equation of motion (1.4), the omitted term being at least two orders of magnitude smaller than the buoyancy term.

Instead of working with the perturbation potential temperature θ' and stratification parameter γ, in the rest of the paper we will work with the buoyancy $b \equiv g\theta'/\theta_r$ and Brunt–Väisälä frequency $N \equiv \sqrt{g\gamma/\theta_r}$. Corresponding to a potential temperature perturbation at the surface θ'_0 is a surface buoyancy $b_0 \equiv g\theta'_0/\theta_r$.

It is convenient to non-dimensionalize variables as

$$(X, Y, Z) \equiv \frac{(x, y, z)}{l_s}, \quad T \equiv \frac{t}{t_s}, \quad \Pi \equiv \frac{p'}{p_s},$$

$$(U, V, W) \equiv \frac{(u, v, w)}{u_s}, \quad B \equiv \frac{b}{b_s}, \quad (1.6)$$

where the length, time, pressure, velocity and buoyancy scales are given, respectively, by

$$l_s \equiv \left(\frac{\nu}{N\sin\alpha}\right)^{1/2}, \quad t_s \equiv \frac{1}{N\sin\alpha}, \quad p_s \equiv \rho_r l_s b_s \cos\alpha,$$

$$u_s \equiv \frac{b_s}{N}, \quad b_s \equiv |b_0|. \quad (1.7)$$

Other non-dimensionalizations are possible, for example, using a length scale l characterizing the width of the surface thermal disturbance. The length, velocity and buoyancy scales adopted in (1.6)–(1.7) characterize the classical 1D Prandtl solution without Coriolis force (p. 374 of Prandtl 1942), which can be written as $u = u_s e^{-z/l_p} \sin(z/l_p)$, $b = b_s e^{-z/l_p} \cos(z/l_p)$, where $l_p \equiv l_s\sqrt{2}/\mathrm{Pr}^{1/4}$. We do not assert that these scales characterize the flow in 2D or 3D Coriolis frameworks better than those from other non-dimensionalizations, but they do facilitate a comparison with classical 1D results.

In terms of the introduced non-dimensional variables, (1.1)–(1.5) become

$$\frac{\partial B}{\partial T} + \mathrm{Re}\mathbf{V} \cdot \nabla B = U - W\cot\alpha + \frac{1}{\mathrm{Pr}}\nabla^2 B, \quad (1.8)$$

$$\frac{\partial U}{\partial T} + \mathrm{Re}\mathbf{V} \cdot \nabla U = -\frac{\partial \Pi}{\partial X}\cot\alpha + \frac{1}{\sqrt{\mathrm{Bu}}}V - B + \nabla^2 U,$$

$$(1.9)$$

$$\frac{\partial V}{\partial T} + \mathrm{Re}\mathbf{V} \cdot \nabla V = -\frac{\partial \Pi}{\partial Y}\cot\alpha - \frac{1}{\sqrt{\mathrm{Bu}}}U + \nabla^2 V,$$

$$(1.10)$$

$$\frac{\partial W}{\partial T} + \mathrm{Re}\mathbf{V} \cdot \nabla W = -\frac{\partial \Pi}{\partial Z}\cot\alpha + B\cot\alpha + \nabla^2 W,$$

$$(1.11)$$

$$\nabla \cdot \mathbf{V} = 0, \quad (1.12)$$

where $\mathbf{V} \equiv U\mathbf{i} + V\mathbf{j} + W\mathbf{k}$ is the non-dimensional velocity vector, and

$$\mathrm{Pr} \equiv \frac{\nu}{\kappa}, \quad \mathrm{Re} \equiv \frac{u_s l_s}{\nu} = \frac{b_s}{(\nu \sin \alpha)^{1/2} N^{3/2}},$$

$$\mathrm{Bu} \equiv \frac{g\gamma \sin^2 \alpha}{\theta_r f^2} = \frac{N^2 \sin^2 \alpha}{f^2} \quad (1.13)$$

are, respectively, the Prandtl number, Reynolds number, and slope Burger number (Garrett, 1991; Garrett *et al.*, 1993). It should be understood that the ∇ and Laplacian ∇^2 operators in (1.8)–(1.12) are non-dimensional.

2. Review of 1D katabatic flow theory with Coriolis effects

Gutman and Malbakhov (1964) derived exact analytical solutions of the equations of motion and thermodynamic energy for local katabatic flow (no interaction with synoptic-scale flow) with the Coriolis force included. Solutions were presented for the temporal development of the flow and the structure of the steady state. The downslope velocity component satisfied a modified (damped) diffusion equation, the solution of which yielded a shallow jet-like flow that in the steady state vanished far above the slope. In contrast, the buoyancy and cross-slope velocity components were each identified as a sum of two different functions, one of which satisfied the modified diffusion equation, and one of which satisfied the classical diffusion equation. This latter equation yielded buoyancy and cross-slope velocity fields that underwent an inexorable upward growth, leading to solutions that did not vanish far above the slope in the steady state (terminal state of the unsteady problem), but approached non-zero constant values.

The non-intuitive result described above was confirmed in studies by Lykosov and Gutman (1972) and Egger (1985) without recourse to the full solution. Following their general approach, we consider the 1D steady-state version of (1.1)–(1.5), expressed in terms of buoyancy, in which there are no flow variations in the x or y directions, so $w = 0$, $\partial p'/\partial x = 0$, $\partial p'/\partial y = 0$, and the x- and y-derivative terms drop from the Laplacians. Eliminating u between (1.1) and (1.3) yields

$$N^2 \nu \sin \alpha \frac{d^2 v}{dz^2} + f\kappa \frac{d^2 b}{dz^2} = 0. \quad (2.1)$$

If $\nu = \kappa = 0$, then (2.1) is identically satisfied, and no further information can be extracted from it (in particular, the conclusions below would not apply). Assuming ν and κ are non-zero, integrate (2.1) twice with respect to z, and impose the remote conditions dv/dz, $db/dz \to 0$ as $z \to \infty$, and slope conditions of no-slip and specified buoyancy b_0. The resulting equation, $N^2 \nu \sin \alpha v + f\kappa b = f\kappa b_0$, together with (1.2) yield the remote ($z \to \infty$) values of b and v as

$$b_\infty = \frac{b_0}{1 + \mathrm{PrBu}}, \quad v_\infty = \frac{\sin \alpha b_0}{f(1 + \mathrm{PrBu})}. \quad (2.2)$$

Thus, neither b nor v vanishes as $z \to \infty$. However, as follows from (1.3), u does vanish as $z \to \infty$. It can be noted that b_∞ and v_∞ do not depend on the values of ν or κ (provided ν and κ are both non-zero!), but only on their ratio Pr. Stiperski *et al.* (2007), perhaps unaware of the previous 1D analytical solutions of katabatic flows with Coriolis effects, considered (1) a steady-state solution equivalent to the asymptotic ($t \to \infty$) solution in Gutman and Malbakhov (1964) for $\mathrm{Pr} = 1$ and shallow slopes, and (2) an approximate transient solution for the cross-slope velocity component that compared favourably with the results of 1D numerical simulation for finite times. These solutions, however, indicated an inexorable upward growth, as in the previous studies. At this point it is worth drawing attention to the fact, not previously noted in the literature, that (2.2) also holds for the more general case where ν and κ are height-dependent eddy viscosity and thermal diffusivity coefficients. This result is obtained in appendix A.

Lykosov and Gutman (1972) and Egger (1985) also showed that if an imposed external downslope pressure gradient force exactly balanced the cross-slope velocity component as $z \to \infty$ (assuming the remote flow to be in geostrophic balance), then the steady-state buoyancy field would vanish as $z \to \infty$. However, Lykosov and Gutman (1972) and Egger (1985) rejected the subsequent results as unphysical, citing unrealistically large cross-slope geostrophic wind speeds (exceeding 100 m s^{-1} for slope angles typical of interior Antarctica) which became singular as the slope angle approached zero. Egger (1985) also drew attention to the deficiency of the 1D model prediction of easterly flow aloft at Antarctic latitudes, which contrasted with the observed cyclonic circulation (This latter criticism points to the more general deficiency of the 1D Cartesian model as applied to the Antarctic circulation (polar vortex). The basic geometry of the Antarctic continent is axisymmetric. Because of this geometry, katabatic flow in the Antarctic is associated with subsidence and corresponding spin-up of a cyclonic polar vortex via the circulation theorem, as schematized in James (1989), Parish and Bromwich (1991) and Parish (1992). Such processes cannot be accounted for in a 1D Cartesian framework. These and other studies have further suggested that a realistic long-time katabatic-flow solution over Antarctica requires eddy transport of polar-vortex angular momentum out of the polar region in order to decrease the magnitude of a polar-vortex-associated pressure-gradient force that would otherwise shut down the katabatic flow. A model of Antarctic katabatic flow including eddy transport would require three dimensions for its description.). A further difficulty with the plausibility of this theory in that the geostrophic wind far away from the surface could not be treated as an arbitrarily imposed (external) forcing but would have to take on a particular value; the geostrophic wind would have to be determined as part of the solution and its value would be tied to the surface buoyancy. Whether such a particular geostrophic wind could arise in nature is questionable.

Egger (1985) also introduced a revised 1D model in which a linear radiative damping term accounting (albeit crudely) for the tendency of the atmosphere to relax toward a reference potential temperature profile was included in the thermodynamic energy equation. Provision for this term led to a steady state in which all flow variables vanished far above the slope without the need for an imposed pressure gradient force. To our knowledge, this revised model is the only 1D local katabatic flow model in which all flow variables exhibit a boundary-layer structure in the steady state. On the other hand, the ad hoc nature of the linear damping term is somewhat unsatisfying.

Similar non-intuitive flow behaviour resulting from the inclusion of the Coriolis force in 1D katabatic models was also found in 1D models of oceanic slope flows (The terms 'downslope' and 'cross-slope' in the oceanic studies correspond to our 'cross-slope' and 'downslope' directions, respectively.) (Thorpe, 1987; Garrett, 1991; MacCready and Rhines, 1991, 1993; Garrett *et al.*, 1993). It was found that: (1) the cross-slope velocity field exhibits a very slow upward adjustment controlled by a diffusion equation, (2) in the steady state, the cross-slope velocity field in the region far above slope attains a (non-zero) value determined by the Coriolis parameter, slope angle, turbulence intensity and buoyancy frequency, and (3) the upslope transport becomes singular for vanishing slope angles. In retrospect, it should not be surprising that similar behaviour arising from the interaction of a stratified rotating fluid with a sloping boundary is found in two different geophysical systems.

A question raised in the oceanic literature relevant to 1D katabatic flow models with Coriolis effects is whether the steady-state solution controlled by the 1D diffusion equation would ever be found in nature. One may speculate that because of the very slow evolution of the cross-slope flow arising from the 1D diffusion equation, additional physical processes, if persistent, may grow in importance in controlling the final structure of the flow. Such processes may break the diffusive nature of the flow, and lead to the development of a well-behaved steady state, as in Egger's (1985) 1D solution when radiative damping is included (radiative time-scale considered by Egger was on the order of 5 days), or may break the 1D symmetry of the flow. The latter effect may arise when the finiteness of real slopes and of surface forcings in the down- and cross-slope directions is taken into account. When considering the structure of katabatic flows with Coriolis effects, one should be attuned to the possibility that processes assumed to be of secondary importance may, if persistent, become vital in controlling the steady state structure, especially far above the slope.

3. Steady-state 1D, 2D and 3D katabatic flows with Coriolis effects

As an extension of the preceding steady-state analysis, we consider the following three idealized classes of katabatic flows:

(1) Flow with doubly-periodic disturbances. All dynamic and perturbation thermodynamic variables are periodic in x and y within a rectangle of finite dimensions: $-L_x \leq x \leq L_x$, $-L_y \leq y \leq L_y$. Although this is generally a 3D flow class, the Prandtl 1D katabatic flow is a special case of (1) since laterally unbounded homogeneous flows are trivially periodic in any domain finite in x and y. Turbulent flow along a uniformly cooled planar surface, the subject of section 4, will also fall into this flow class.

(2) Flow with 3D isolated disturbances. All dynamic and perturbation thermodynamic variables vanish as $|x| \to \infty$ and as $|y| \to \infty$.

(3) Flow with singly-periodic disturbances. All dynamic and perturbation thermodynamic variables are periodic in the downslope direction x, and vanish as $|y| \to \infty$. An important sub-class, considered in sections 5 and 6, is 2D (y–z) flow induced by a strip of negative surface buoyancy running down the slope. The surface buoyancy is negative within a strip of finite width in the cross-slope direction, and is zero outside of this strip. Variables in such flows are independent of x, and so are trivially periodic in x. Another sub-class (not studied here) is 2D (x–z) flow in which a cold strip runs across the slope, all variables being independent of y.

Although these classes are fairly general, they do not include flows subjected to a constant perturbation pressure gradient force, such as would be required to balance a synoptic-scale geostrophic wind. A constant perturbation pressure gradient would be associated with a linearly varying p' field which neither vanishes as x or y approaches infinity nor is periodic. Accordingly, the (1)–(3) flows are local in the sense that they are not interacting with larger-scale flows.

Now integrate the steady-state versions of (1.1)–(1.5) over a 2D x–y domain particular to the flow class: a rectangle $-L_x \leq x \leq L_x$, $-L_y \leq y \leq L_y$ for the doubly-periodic disturbance (1), an infinite x–y domain, $\lim_{L_x \to \infty} -L_x < x < L_x$, $\lim_{L_y \to \infty} -L_y < y < L_y$, for the isolated disturbance (2), and a finite x-domain $-L_x \leq x \leq L_x$ and infinite y-domain, $\lim_{L_y \to \infty} -L_y < y < L_y$, for a strip running down the slope (3). Writing all advection terms in flux form ($\mathbf{v} \cdot \nabla S = \nabla \cdot (\mathbf{v}S)$, where S is a generic scalar), and applying the divergence theorem to the integrals of those terms, yields lateral boundary integrals which vanish because of the boundary conditions in (1)–(3). Similarly it can be shown that the x and y derivative terms in the Laplacians integrate to zero.

The integrated form of (1.5) becomes $d\overline{w}/dz = 0$, where an overbar denotes an x–y integral. Integrating $d\overline{w}/dz = 0$ with respect to z, and imposing the impermeability condition ($w = 0$ along the slope so $\overline{w} = 0$ along the slope), we see that $\overline{w}(z)$ is identically zero, although nonlinear terms like $\overline{wS}$ may not be zero. The

$x-y$ integrated forms of (1.1)–(1.3) appear as

$$\frac{\mathrm{d}}{\mathrm{d}z}(\overline{wb}) = N^2 \sin\alpha\overline{u} + \kappa\frac{\mathrm{d}^2\overline{b}}{\mathrm{d}z^2}, \qquad (3.1)$$

$$\frac{\mathrm{d}}{\mathrm{d}z}(\overline{wu}) = f\overline{v} - \overline{b}\sin\alpha + \nu\frac{\mathrm{d}^2\overline{u}}{\mathrm{d}z^2}, \qquad (3.2)$$

$$\frac{\mathrm{d}}{\mathrm{d}z}(\overline{wv}) = -f\overline{u} + \nu\frac{\mathrm{d}^2\overline{v}}{\mathrm{d}z^2}. \qquad (3.3)$$

Equations (3.1) and (3.3) reveal that if flow variables approach constant (zero or non-zero) values as $z \to \infty$ then the remote ($z \to \infty$) $x-y$ integrated downslope velocity $\overline{u}_\infty$ must be zero. However, this does not mean that u_∞ itself must be zero, only that it integrates to zero. Indeed, in the numerical simulations of 2D strip flow (section 6) a purely horizontal along-isentrope streaming motion developed far above the slope, with an anti-symmetric (with respect to centre of strip) upslope/toward-boundary-layer flow on one side of the strip, and a downslope/away-from-boundary-layer flow on the other side of the strip.

To elucidate the behaviour of $\overline{v}$ and $\overline{b}$, first eliminate $\overline{u}$ between (3.1) and (3.3), obtaining

$$\frac{\mathrm{d}}{\mathrm{d}z}\overline{w(fb + N^2\sin\alpha v)} = \frac{\mathrm{d}^2}{\mathrm{d}z^2}(f\kappa\overline{b} + N^2\nu\sin\alpha\overline{v}). \qquad (3.4)$$

Integration of (3.4) with respect to z (with $\partial b/\partial z$, $\partial v/\partial z \to 0$ as $z \to \infty$) yields

$$\overline{w(fb + N^2\sin\alpha v)} - \overline{w(fb + N^2\sin\alpha v)}\Big|_\infty$$
$$= \frac{\mathrm{d}}{\mathrm{d}z}(f\kappa\overline{b} + N^2\nu\sin\alpha\overline{v}). \qquad (3.5)$$

Integration of (3.5) with respect to z then yields

$$\int_0^z \left(\overline{w(fb + N^2\sin\alpha v)} - \overline{w(fb + N^2\sin\alpha v)}\Big|_\infty\right)$$
$$\mathrm{d}z' = f\kappa\overline{b} + N^2\nu\sin\alpha\overline{v} - f\kappa\overline{b}_0, \qquad (3.6)$$

where lower boundary conditions of impermeability, no slip and specified buoyancy have been imposed. If we consider linear dynamics, then the left-hand side of (3.6) is neglected, and evaluation of (3.6) as $z \to \infty$ shows that $f\overline{b}_\infty + N^2\mathrm{Pr}\sin\alpha\overline{v}_\infty = f\overline{b}_0$. Comparing this result with the linearized version of (3.2) as $z \to \infty$ yields the same formulae as in (2.2) but involving the $x-y$ integrals $\overline{b}_\infty$, $\overline{v}_\infty$ and $\overline{b}_0$. We conclude that if $\overline{b}_0$ is non-zero then $\overline{b}_\infty$ and $\overline{v}_\infty$ are also non-zero.

The implication of the above result varies with the flow class. For a doubly-periodic flow (1), where a finite $x-y$ domain is considered, a non-zero integral $\overline{b}_\infty$ is associated with a non-zero $x-y$-average $L_x^{-1}L_y^{-1}\overline{b}_\infty$. In this case, b_∞ does not vanish as $z \to \infty$, and the disturbance is felt at infinity. The 1D flow analysed by Egger (1985) and others is a special case of this flow type. However, for flow induced by a 2D cold strip running down the slope,

a special case of (3) in which all variables are independent of x, we must look more closely at the non-averaged equations. Taking the z-derivative of (1.3), and assuming $\partial u/\partial z$, $\partial v/\partial z \to 0$ as $z \to \infty$, yields $\partial^2 p'/(\partial y\partial z) \to 0$ as $z \to \infty$. The equation resulting from taking the y-derivative of (1.4), assuming hydrostatic conditions as $z \to \infty$, then yields $\partial b/\partial y \to 0$ as $z \to \infty$. However, since b vanishes as $|y| \to \infty$, b must vanish far above the slope for all y, that is, $b_\infty \to 0$. This seemingly contradicts the previous result that $\overline{b}_\infty$ is not zero; however, the results may be reconciled by noting that as $z \to \infty$ a function can vanish even though its $x-y$ integral does not vanish (As an example, consider $F \equiv z^{-1}\exp(-ay^2/z^2)$, where a is a positive constant. As $z \to \infty$, this function vanishes, but its $x-y$ integral $\overline{F} = \int_{-L_x}^{L_x}\int_{-\infty}^{\infty} F\,\mathrm{d}y\mathrm{d}x = 4L_x a^{-1/2}\int_0^\infty \exp(-\chi^2)\mathrm{d}\chi = 2L_x\sqrt{\pi/a}\,\mathrm{erf}(\infty) = 2L_x\sqrt{\pi/a}$, which is independent of z, does not vanish.). The vanishing of v as $z \to \infty$ follows from (1.5) and the condition that $v \to 0$ as $|y| \to \infty$. It can also be noted that since $b \to 0$ as $z \to \infty$, (1.4) yields $\partial p'/\partial z \to 0$ as $z \to \infty$ (provided flow is hydrostatic as $z \to \infty$). Similarly, it can be shown for an isolated disturbance (2) that $b_\infty \to 0$ as $z \to \infty$, even though $\overline{b}_\infty$ is not zero. In this case, however, it is not clear that v_∞ vanishes for all x and y since the possibility of a geostrophic adjustment leading to a balance between the v and $\partial p'/\partial x$ terms far above the slope cannot be ruled out.

Returning to the doubly-periodic flow case (1) and to (3.6) with the nonlinear terms retained, one obtains an integral condition that should be satisfied if b and v were to vanish as $z \to \infty$:

$$\int_0^\infty \left(\overline{w(fb + N^2\sin\alpha v)} - \overline{w(fb + N^2\sin\alpha v)}\Big|_\infty\right)$$
$$\mathrm{d}z' = -f\kappa\overline{b}_0. \qquad (3.7)$$

Although the presence of the nonlinear terms in the left-hand side of (3.7) offers the possibility that a self-adjustment process might occur in turbulent flows such that flow variables vanish far above the slope, there is no reason to expect this to take place. Indeed, a numerical simulation (section 4) showed that in a homogeneous turbulent katabatic flow there was an inexorable upward growth of the buoyancy and cross-slope wind with height as in the 1D laminar case.

4. Numerical simulation of turbulent katabatic flow

In this section we present direct numerical simulation (DNS) results for laminar and turbulent katabatic flows along a uniformly cooled sloping surface, a class (1) flow in section 3. The atmosphere is initially quiescent, and flow is induced by the sudden imposition (at $T = 0$) and maintenance of a constant surface buoyancy. If the surface buoyancy is sufficiently strong (large Re, see (1.13)), the flow transits at an early stage from a laminar regime to a turbulent regime. Since the turbulence is explicitly

Copyright © 2008 Royal Meteorological Society

Q. J. R. Meteorol. Soc. **134**: 353–370 (2008)

simulated in DNS, there is no need for closure assumptions concerning the values of the eddy viscosity and diffusivity coefficients. The ν and κ coefficients appearing in the governing equations of DNS are intended to be molecular coefficients. However, because the computational expense and memory requirements for realistic turbulent katabatic simulations running over several inertial periods are prohibitive, our turbulence simulations were restricted to Reynolds numbers of order 10^4, compared with atmospheric Reynolds numbers several orders of magnitude larger. Accordingly, our results should be used for no more than a qualitative illustration of the larger-scale turbulence behaviour.

The numerical procedures are patterned on the works of Nieuwstadt (1990), Fedorovich *et al.* (2001), and Shapiro and Fedorovich (2004, 2006), and will only be briefly summarized here. The model equations are (1.8)–(1.11), together with an elliptic equation (Poisson equation) for the perturbation pressure that results from taking the X-, Y-, and Z- derivatives of (1.9), (1.10), and (1.11), respectively, adding the resulting equations together, and applying (1.12). The model equations are discretized on a staggered Cartesian (X, Y, Z) grid with a uniform spacing in a rectangular domain. The spatial derivatives are discretized with second-order finite difference expressions. The prognostic variables are calculated by integrating (1.8)–(1.11) with respect to time using a leap-frog scheme with a weak Asselin filter. The filter constant is 0.25, which provides a maximum Courant number of 0.75 with the second-order central differencing in space. The elliptic equation for the perturbation pressure is solved at each time step with a Fast Fourier Transform technique over X–Y planes, and tri-diagonal matrix inversion in the Z direction. On the slope $(Z = 0)$, no-slip and impermeability conditions are imposed on the velocity components, the surface buoyancy is prescribed, and the slope-normal derivative of Π is calculated as a residual from the slope-normal equation of motion. At the top of the computational domain, the normal gradients of all variables are set to zero. Periodic boundary conditions are imposed for all variables on the four lateral boundaries, the X–Z and Y–Z slope-normal planes.

For the experiments described in this section, the slope angle is $\alpha = 3°$. For the experiment with the Coriolis force, Bu = 1, and f is taken positive, while Bu = ∞ for the experiment without the Coriolis force. In the turbulent flow simulations, the Reynolds number is set to Re = $3000/\sqrt{\sin 3°} \approx 13\,000$, while for the laminar simulations, Re = $1/\sqrt{\sin 3°} \approx 4$. The grid spacing in the simulations is chosen to satisfy resolvability criteria for the smallest scales of motion. Values of the dimensionless spatial grid increments $(\Delta X = \Delta Y = \Delta Z)$ were 0.05 and 0.25 in the laminar and turbulent flow simulations, respectively. The time step is adaptively determined so that the stability criteria associated with the advection (Courant–Friedrichs–Lewy criterion) and diffusion operators are satisfied.

Numerical results for a Prandtl-type laminar run without Coriolis force are presented in Figure 2. The boundary-layer character of the downslope wind and buoyancy fields is well-established by time $T = 2$ (dimensional time, of order $2(N \sin \alpha)^{-1}$). A longer-time simulation (not shown) indicates that the solution near the end time in Figure 2 is very close to the steady-state solution. This steady state is approached as a low-frequency gravity wave with dimensional frequency $N \sin \alpha$ gradually decays with time. In the laminar simulation with the Coriolis force (Figure 3), the downslope wind is qualitatively similar to that obtained in the simulation without the Coriolis force. However, the buoyancy and cross-slope wind in the simulation with the Coriolis force continue to grow upward with time. A longer-time simulation extending over 20 oscillation periods (not shown) indicated that the buoyancy and cross-slope wind fields had attained a steady state near the slope, but were
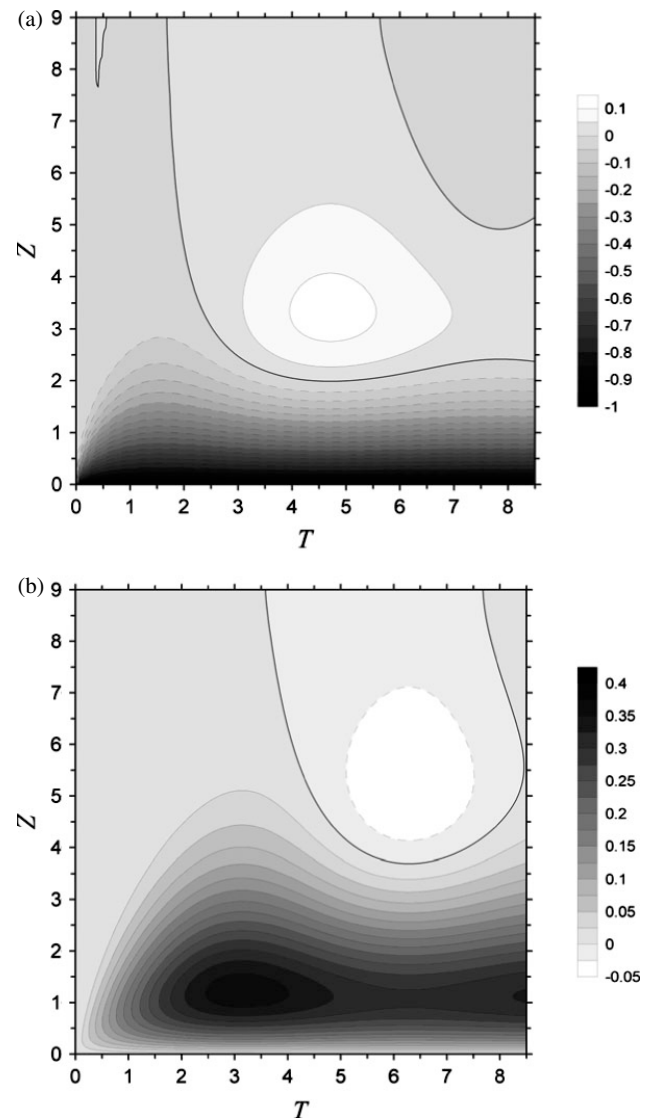

Figure 2. Evolution of (a) buoyancy B and (b) downslope velocity U in the laminar flow along a uniformly cooled slope in the absence of Coriolis force (Bu = ∞). Negative contours are dashed. Zero contours are marked with bold solid lines.
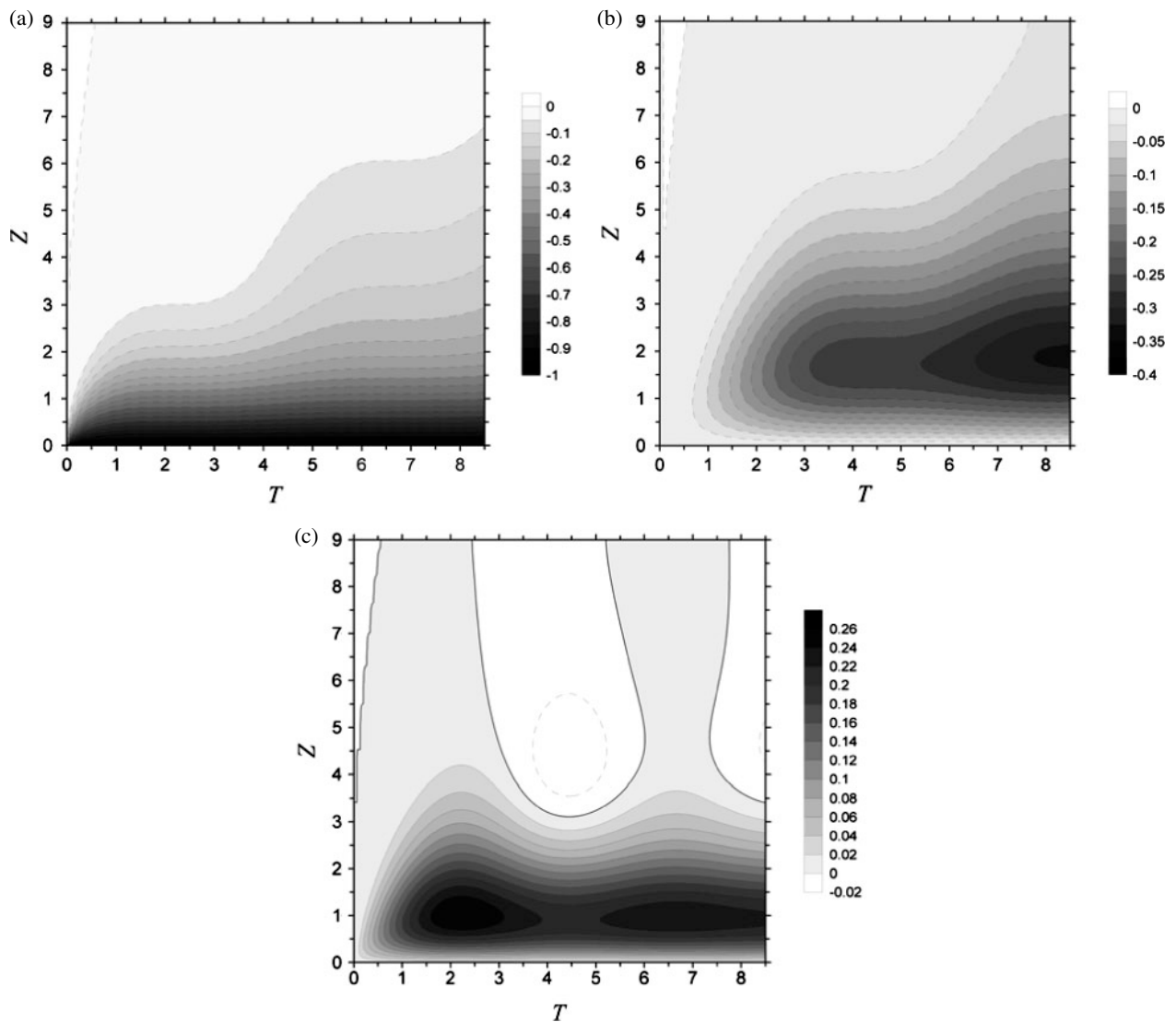
Figure 3. Evolution of (a) buoyancy B, (b) cross-slope velocity V, and (c) downslope velocity U in the laminar flow along a uniformly cooled slope in the presence of Coriolis force (Bu $= 1$). Negative contours are dashed. Zero contours are marked with bold solid lines.

still slowly growing in value far above the slope. These results are consistent with the solutions of Gutman and Malbakhov (1964), Lykosov and Gutman (1972) and Egger (1985).

Numerical results from the turbulent simulations are presented in Figures 4 and 5. Comparing the results from the turbulent and laminar flow simulations without Coriolis force (Figures 2 and 4), we first note that the boundary layer in the turbulent flow is much thicker than in the laminar flow (note change of scale of Z axis), but in both cases the flows are approaching steady states. Also apparent are high-frequency oscillations with dimensional frequency N. A lower-frequency oscillation with dimensional frequency $N \sin \alpha$ may also be present, but a longer simulation would be required to confirm it. However, in experiments with steeper slopes and no Coriolis force (not shown), several periods of this low-frequency wave were apparent before the end of the simulation. Comparing the laminar and turbulent simulations with the Coriolis force (Figures 3

and 5), we see that the cross-slope velocity and buoyancy fields exhibit a similar inexorable growth with distance above the slope in both cases. Apparently there is no self-adjustment process in the turbulent flow that allows (3.7) to be satisfied. Although this result is obtained for a Reynolds number far smaller than would be found in nature, the fact that qualitatively similar behaviour appears in a laminar flow and its turbulent counterpart suggests that the gross behaviour may be fundamental.

A recent study by Kavčič and Grisogono (2007) suggested that steady-state cross-slope velocity and buoyancy fields could vanish far above the slope in a 1D framework if suitable profiles of eddy viscosity and diffusivity were adopted. However, in view of our DNS results and the results summarized in section 2, which suggest that even small background values of ν and κ should profoundly change the structure of the buoyancy and cross-slope velocity far above the slope in the steady state, and the results in appendix
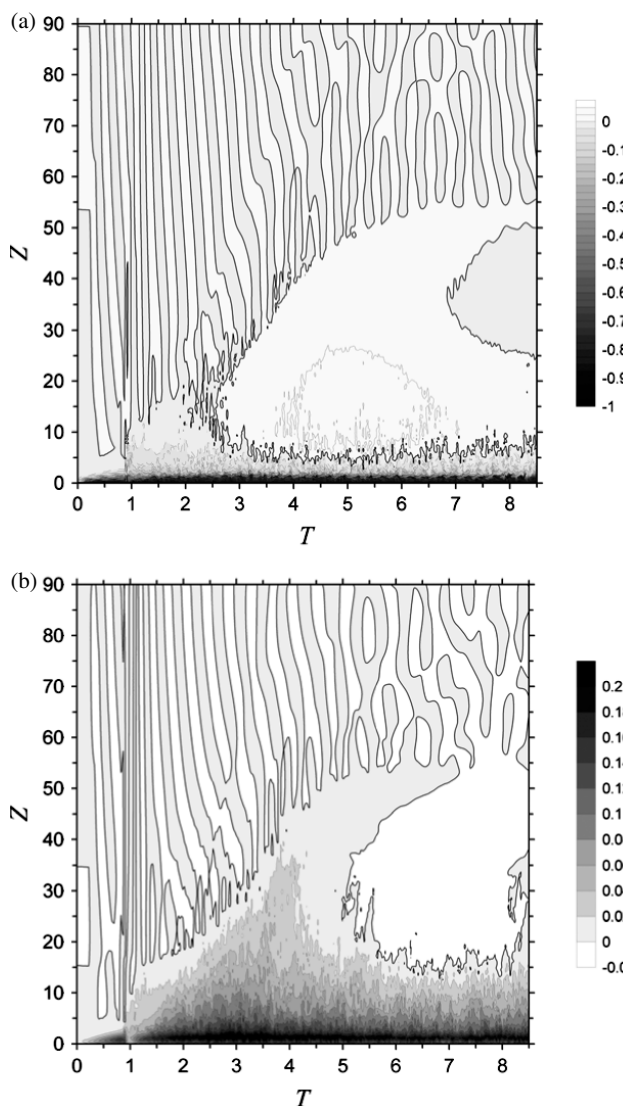
Figure 4. As in Figure 2 but for the turbulent katabatic flow.

A concerning general height-dependent mixing coefficients, we have to question the conclusions of that latter study. It is likely that a steady state had not yet been obtained for the results presented in that study, and that a slow (but inexorable) upward growth of the solution was occurring. Indeed, inspection of panels (c) and (d) of Figure 3 of that paper show that the numerical solution for the cross-slope velocity was slowly evolving.

5.   Linear analysis of 2D katabatic flow

In this section, a partial (limited) linear analysis of (1.8)–(1.12) with a Prandtl number of unity is conducted for steady-state katabatic flow with cross-slope (Y) inhomogeneity and Coriolis force. The approach is similar to that of the Egger (1981) and Kondo (1984) analyses of slope flow with downslope (X) inhomogeneity without Coriolis force. The flow is induced by a surface buoyancy $B(Y, 0)$ that is constant in a strip of finite Y-width,

and decays to zero as $Y \rightarrow \pm\infty$. All flow variables are independent of X. The U, V and B variables are considered to vanish as $Y \rightarrow \pm\infty$, and their Z-derivatives are considered to vanish as $Z \rightarrow \infty$. No assumptions are made for the remote behaviour of Π since our analysis is based on a vorticity/stream-function formulation in which Π does not appear. However, we anticipate that it may not be possible for U, V and B themselves to actually vanish as $Z \rightarrow \infty$; some variables might approach non-zero values. Elucidating the behaviour of the flow far above the slope is one of the main objectives of this analysis.

5.1.   Reduction of the governing equations

With the flow considered homogeneous in the X direction, all X-derivative terms drop from the linearized versions of (1.8)–(1.12), including the downslope pressure gradient force in (1.9). We also consider length scales of cross-slope inhomogeneity large enough that the $\partial^2/\partial Y^2$ terms are much smaller than the $\partial^2/\partial Z^2$ terms in the Laplacians and can be safely neglected (boundary-layer type approximation). Because of the shallowness of katabatic flows, such an approximation should be valid everywhere except for the vicinity of strong along- or cross-slope variations of flow variables, should they occur. Moreover, because of the presumed shallowness of the flow, we use the hydrostatic approximation for the slope-normal equation of motion. With these considerations, the steady linearized versions of (1.8)–(1.12) with $\mathrm{Pr} = 1$ (chosen for convenience) appear as

$$0 = U - W\cot\alpha + \frac{\partial^2 B}{\partial Z^2}, \tag{5.1}$$

$$0 = \frac{1}{\sqrt{\mathrm{Bu}}}V - B + \frac{\partial^2 U}{\partial Z^2}, \tag{5.2}$$

$$0 = -\frac{\partial \Pi}{\partial Y}\cot\alpha - \frac{1}{\sqrt{\mathrm{Bu}}}U + \frac{\partial^2 V}{\partial Z^2}, \tag{5.3}$$

$$0 = -\frac{\partial \Pi}{\partial Z} + B, \tag{5.4}$$

$$0 = \frac{\partial V}{\partial Y} + \frac{\partial W}{\partial Z}. \tag{5.5}$$

We eliminate V and W in (5.1)–(5.5) in favour of a stream function Ψ defined by

$$V = \frac{\partial \Psi}{\partial Z}, \quad W = -\frac{\partial \Psi}{\partial Y}. \tag{5.6}$$

We also eliminate Π from this system by subtracting the Y-derivative of (3.4) from the Z-derivative of (5.3). Collecting results, (5.1)–(5.4) reduce to the eighth-order system:

$$0 = U + \frac{\partial \Psi}{\partial Y}\cot\alpha + \frac{\partial^2 B}{\partial Z^2}, \tag{5.7}$$

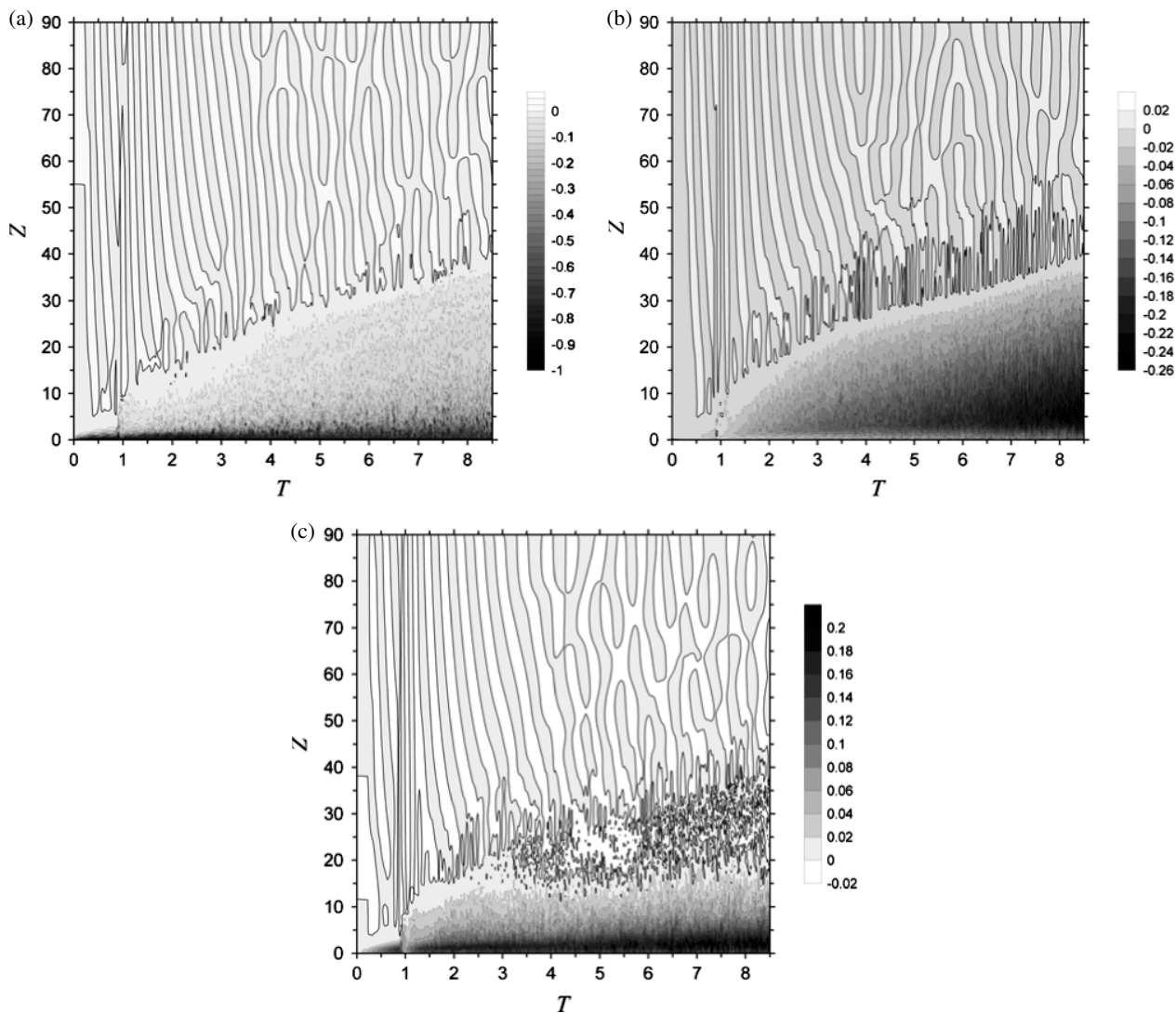Figure 5. As in Figure 3 but for the turbulent katabatic flow.

$$0 = \frac{1}{\sqrt{\text{Bu}}}\frac{\partial \Psi}{\partial Z} - B + \frac{\partial^2 U}{\partial Z^2}, \qquad (5.8)$$

$$0 = -\cot\alpha \frac{\partial B}{\partial Y} - \frac{1}{\sqrt{\text{Bu}}}\frac{\partial U}{\partial Z} + \frac{\partial^4 \Psi}{\partial Z^4}, \qquad (5.9)$$

with (5.5) satisfied identically. Equation (5.9) is a down-slope vorticity equation, with the first, second and third terms accounting, respectively, for baroclinic generation, tilting of planetary vorticity in the downslope direction, and slope-normal diffusion of downslope vorticity.

We now inspect (5.7)–(5.9) far above the slope ($Z \rightarrow \infty$), where the Z-derivatives of the buoyancy and velocity fields are supposed to vanish. Equation (5.9) reveals that $\partial B/\partial Y \rightarrow 0$, that is, B becomes independent of Y far above the slope. However, since $B \rightarrow 0$ as $Y \rightarrow \pm\infty$, we see that B itself vanishes far above the slope. Equation (5.8) then shows that $V (= \partial \Psi/\partial Z)$ must vanish, while (5.7) indicates that U must compensate the term containing $\partial \Psi/\partial Y (= -W)$. These two terms account for the downslope and slope-normal advection of environmental potential temperature, respectively. Their

sum is the true vertical advection of environmental potential temperature, as can be seen by tracing the two terms back to the thermodynamic energy equation (1.1) and recalling that $W \cos\alpha - U \sin\alpha$ is the true vertical velocity field. Since this sum approaches zero far above the slope, a non-zero U would be associated with a purely horizontal streaming motion parallel to the environmental isentropes. We also see from (5.3) that a non-zero U far above the slope would be associated with a non-zero $\partial \Pi/\partial Y$, a balance of these two terms indicating a geostrophic balance. Since the initial state was of no motion and no imposed pressure gradient, the presence of non-zero U and $\partial \Pi/\partial Y$ far above the slope in the steady state would imply that a geostrophic adjustment process had occurred. As will be shown below and confirmed by numerical simulations (section 6), a non-zero remote value of U (with near-zero remote values for B and V) in the steady state is a feature of this strip flow. In contrast, far above the slope in the 1D case (section 2), the steady state B and V fields are non-zero, while U is zero.

The eighth-order system (5.7)–(5.9) can be reduced to a sixth-order system. Adding together (5.9), the equation resulting from taking $1/\sqrt{Bu}$ times the Z-derivative of (5.7), and the equation resulting from taking $-\cot\alpha$ times the Y-derivative of (5.8), yields $\partial^2 G/\partial Z^2 = 0$, where $G \equiv 1/\sqrt{Bu}\,\partial B/\partial Z + \partial^2\Psi/\partial Z^2 - \cot\alpha\,\partial U/\partial Y$. Integrating $\partial^2 G/\partial Z^2 = 0$ twice yields $G = C + DZ$, where C and D are functions of integration, possibly functions of Y. The vanishing of the Z-derivatives of all variables far above the slope implies $D = 0$. We are tempted to take $C = 0$ as this would force $\partial U/\partial Y$ (and hence U) to vanish far above the slope. However, as we will see in subsection 5.4, we are not at liberty to specify C, as that would lead to an over-determined system. Rather, C must depend on the other parameters of the problem. We write $G = C$ as

$$\frac{1}{\sqrt{Bu}}\frac{\partial B}{\partial Z} + \frac{\partial^2\Psi}{\partial Z^2} - \cot\alpha\frac{\partial U}{\partial Y} = C, \qquad (5.10)$$

and note that since (5.10) together with (5.7) and (5.8) can be used to derive (5.9), we may use the sixth-order system (5.7), (5.8), (5.10) in place of the eighth-order system (5.7)–(5.9).

Taking the Fourier transform of (5.7), (5.8), (5.10) with respect to Y yields

$$\hat{U} + iK\cot\alpha\,\hat{\Psi} + \frac{d^2\hat{B}}{dZ^2} = 0, \qquad (5.11)$$

$$\frac{1}{\sqrt{Bu}}\frac{d\hat{\Psi}}{dZ} - \hat{B} + \frac{d^2\hat{U}}{dZ^2} = 0, \qquad (5.12)$$

$$\frac{1}{\sqrt{Bu}}\frac{d\hat{B}}{dZ} + \frac{d^2\hat{\Psi}}{dZ^2} - iK\cot\alpha\,\hat{U} = \hat{C}, \qquad (5.13)$$

where K is a cross-slope wave number, and a hat denotes a Fourier-transformed variable. For example, $\hat{\Psi} \equiv (2\pi)^{-1/2}\int_{-\infty}^{\infty} e^{-iKY}\Psi dY$.

A particular solution of (5.11)–(5.13) is identified as

$$\hat{U}_p = i\frac{\hat{C}\tan\alpha}{K}, \quad \hat{\Psi}_p = -\frac{\hat{C}\tan^2\alpha}{K^2}, \quad \hat{B}_p = 0. \quad (5.14)$$

The general solution can be written as the sum of this particular solution and the linearly independent homogeneous parts:

$$\hat{U} = \hat{U}_p + \Sigma\tilde{U}e^{MZ}, \quad \hat{\Psi} = \hat{\Psi}_p + \Sigma\tilde{\Psi}e^{MZ},$$
$$\hat{B} = \Sigma\tilde{B}e^{MZ}, \qquad (5.15)$$

where the constant M needs to be determined. The amplitude parameters $\tilde{U}$, $\tilde{\Psi}$, $\tilde{B}$ appearing in (5.15) are independent of Z. Applying (5.15) in (5.11)–(5.13) yields the matrix equation

$$\begin{pmatrix} M^2 & 1 & iK\cot\alpha \\ -1 & M^2 & M/\sqrt{Bu} \\ M/\sqrt{Bu} & -iK\cot\alpha & M^2 \end{pmatrix}\begin{pmatrix} \tilde{B} \\ \tilde{U} \\ \tilde{\Psi} \end{pmatrix} = \begin{pmatrix} 0 \\ 0 \\ 0 \end{pmatrix}.$$
$$(5.16)$$

Non-trivial solutions of (5.16) only exist for a vanishing determinant, that is, for M satisfying

$$M^6 + (1 + 1/Bu)M^2 - K^2\cot^2\alpha = 0. \qquad (5.17)$$

The placement of M in (5.15) identifies it as a reciprocal vertical length scale. Of the six roots of (5.17), we reject the roots with positive real part to avoid unbounded growth far above the slope. The three physically acceptable roots of (5.17) are obtained in appendix B as (B9)–(B11). To determine the character of the buoyancy B and cross-slope flow $V(= \partial\Psi/\partial Z)$ far above the slope, we are primarily interested in the smallest of these roots as it corresponds to the largest of the vertical length scales. In contrast, (5.15) indicates that the behaviour of the downslope velocity U and slope-normal velocity $W(= -\partial\Psi/\partial Y)$ far above the slope is controlled by $\hat{C}$.

In the following, we assume the qualitative behaviour of the cross-slope velocity and buoyancy solutions of (5.15) far above the slope can be inferred from the solutions M of (5.17) corresponding to a dominant wave number K. This assumption is valid only if the Fourier-transformed functions are narrow-banded in K, which should be the case for broad disturbances. Since the dominant K should be inversely related to the characteristic cross-slope width of the flow, one might anticipate the dominant K should be inversely related to the cross-slope width of the cold strip. However, the question of how wide the flow should be will not be addressed here. Rather, we assume that a dominant K characterizes the flow, and that a dominant vertical length scale associated with it is the smallest of the three physically acceptable roots of (5.17).

In subsections 5.2 and 5.3 we consider simple approximate solutions of (5.17) appropriate for small and large values of the dominant cross-slope wave number K. More specifically, the approximations are obtained for small ($\ll 1$) or large ($\gg 1$) values of the K-dependent parameter ε defined in (B5). The form of ε suggests that a useful reference wave number K_{ref} for these approximations is

$$K_{ref} \equiv \tan\alpha(1 + 1/Bu)^{3/4}, \qquad (5.18)$$

in terms of which ε becomes $\varepsilon = (K/K_{ref})^2 3^{3/2}/2$.

5.2. Small-K approximation

To obtain approximate solutions for M for small K ($K \ll K_{ref}$ so $\varepsilon \ll 1$), make repeated use of binomial approximations in (B9)–(B11), obtaining

$$M_1 = -\frac{K\cot\alpha}{\sqrt{1 + 1/Bu}}, \quad M_2 = -\left(\frac{1+i}{\sqrt{2}}\right)(1 + 1/Bu)^{1/4},$$

$$M_3 = M_2^*, \quad (K \ll K_{ref}) \qquad (5.19)$$

Table I. Vertical length scale $|M_1|^{-1}l_s$ versus slope angle α.

α (°)	Bu	l_s (m)	K_{ref}	$K \, (= kl_s)$	$|M_1|^{-1}l_s$ (m)
0.6	1.1	97.7	1.7×10^{-2}	3.9×10^{-3}	360
1.0	3.0	75.7	2.2×10^{-2}	3.0×10^{-3}	510
2.0	12.2	53.5	3.7×10^{-2}	2.1×10^{-3}	970
3.0	27.4	43.7	5.4×10^{-2}	1.7×10^{-3}	1340
4.0	48.7	37.9	7.1×10^{-2}	1.5×10^{-3}	1760
5.0	76.0	33.9	8.8×10^{-2}	1.4×10^{-3}	2200

M_1 obtained from small-K formula (5.19). $N = 0.01$ s^{-1}, $\nu = 1$ m^2 s^{-1}, $f = 10^{-4}$ s^{-1}, $k = 4 \times 10^{-5}$ m^{-1}. See text for details.

where an asterisk (*) denotes complex conjugation. Of these roots, only M_1 depends on K. Since the magnitudes of M_1/M_2 and M_1/M_3 are of the order K/K_{ref} ($\ll 1$), the vertical length scale associated with M_1 is larger than that associated with M_2 or M_3. We note that as $K \to 0$, M_1 vanishes, and the vertical length scale M_1^{-1} becomes infinite. A flow with $K \to 0$ is equivalent to a flow for which all Y-derivative terms in (5.1)–(5.5) vanish and consequently W is zero everywhere (from mass conservation and the impermeability condition). This is the traditional 1D scenario (e.g. Egger, 1985), for which it is known that V and B do not vanish at infinity. Now consider an example with $N = 0.01$ s^{-1}, $\nu = 1$ m^2 s^{-1}, $f = 10^{-4}$ s^{-1}, and the dominant cross-slope length scale is $k^{-1} = 25$ km ($k = 4 \times 10^{-5}$ m^{-1}). The dominant dimensional vertical length scale $|M_1|^{-1}l_s$ corresponding to these values and to a range of slope angles is presented in Table I. The dominant values of K ($= kl_s$) are much less than K_{ref}, implying the validity of (5.19) in this example.

5.3. Large-K approximation

To approximate the roots (B9)–(B11) for large K ($\varepsilon \gg 1$; $K \gg K_{ref}$), rewrite the roots in terms of $1/\varepsilon$ ($\ll 1$) and impose binomial approximations, obtaining

$$M_1 = -(K \cot\alpha)^{1/3}, \quad M_2 = -\left(\frac{1 + i\sqrt{3}}{2}\right)(K \cot\alpha)^{1/3},$$

$$M_3 = M_2^*. \quad (K \gg K_{ref}) \tag{5.20}$$

These three roots are of similar magnitude, independent of Bu, and increase as the third root of K. Accordingly, the dominant vertical length scale is independent of Bu and increases as the third root of the dominant cross-slope length scale: $M^{-1} \propto (k^{-1})^{1/3}$. For an example, consider $N = 0.01$ s^{-1}, $f = 10^{-4}$ s^{-1}, $\nu = 1$ m^2 s^{-1}, $\alpha = 1°$ (so $l_s \cong 75.7$ m, $K_{ref} \cong 2.2 \times 10^{-2}$) and a dominant cross-slope length scale $k^{-1} = 500$ m (so $k = 2.0 \times 10^{-3}$ m^{-1}, $K = kl_s \cong 1.5 \times 10^{-1} \gg K_{ref}$). From (5.20), the corresponding dimensional vertical length scale is $|M_1|^{-1}l_s \cong 37$ m.

5.4. Closure

From the analysis of subsection 5.1 we see that solutions of (5.11)–(5.13) are of the form

$$\hat{B} = \tilde{B}_1 \exp(M_1 Z) + \tilde{B}_2 \exp(M_2 Z) + \tilde{B}_3 \exp(M_3 Z), \tag{5.21}$$

$$\hat{U} = i\frac{\hat{C} \tan\alpha}{K} + \tilde{U}_1 \exp(M_1 Z) + \tilde{U}_2 \exp(M_2 Z) + \tilde{U}_3 \exp(M_3 Z), \tag{5.22}$$

$$\hat{\Psi} = -\frac{\hat{C}\tan^2\alpha}{K^2} + \tilde{\Psi}_1 \exp(M_1 Z) + \tilde{\Psi}_2 \exp(M_2 Z) + \tilde{\Psi}_3 \exp(M_3 Z). \tag{5.23}$$

Applying (5.21)–(5.23) in (5.11)–(5.13) yields three sets of three equations, one set for each M. However, the three equations in each set are not independent since the matrix equation associated with each set is essentially (5.16), whose determinant vanishes. Discarding one equation from each set leaves six independent equations. To close the system, impose slope ($Z = 0$) boundary conditions of specified buoyancy, impermeability, and no slip for U and V ($= \partial\Psi/\partial Z$) in (5.21)–(5.23) and the Z-derivative of (5.23), obtaining

$$\hat{B}_0 = \tilde{B}_1 + \tilde{B}_2 + \tilde{B}_3, \tag{5.24}$$

$$\frac{\hat{C} \tan^2\alpha}{K^2} = \tilde{\Psi}_1 + \tilde{\Psi}_2 + \tilde{\Psi}_3, \tag{5.25}$$

$$-i\frac{\hat{C} \tan\alpha}{K} = \tilde{U}_1 + \tilde{U}_2 + \tilde{U}_3, \tag{5.26}$$

$$0 = M_1\tilde{\Psi}_1 + M_2\tilde{\Psi}_2 + M_3\tilde{\Psi}_3, \tag{5.27}$$

where $\hat{B}_0$ is the Fourier-transformed surface buoyancy $B(Y, 0)$.

We thus obtain a closed system of ten equations in ten unknowns ($\hat{C}$, $\tilde{U}_1$, $\tilde{U}_2$, $\tilde{U}_3$, $\tilde{B}_1$, $\tilde{B}_2$, $\tilde{B}_3$, $\tilde{\Psi}_1$, $\tilde{\Psi}_2$, $\tilde{\Psi}_3$). Specifying $C = 0$ ($\hat{C} = 0$), would result in an over-determined system of ten equations in nine unknowns, with no solution possible. Since $\hat{C}$ is generally non-zero, (5.22) and (5.23) show that $\hat{U}$ and $\hat{\Psi}$ do not vanish far above the slope, although their Z-derivatives do vanish. Accordingly, far above the slope, U, $\partial U/\partial Y$ and $W = -\partial\Psi/\partial Y$ do not vanish, but $V = \partial\Psi/\partial Z$ and B do vanish. In view of the results described in subsection 5.1 from the analysis of (5.7)–(5.9), these non-zero U and W fields must be associated with a purely horizontal streaming motion parallel to the environmental isentropes.

Although the procedure for completing the analytical solution of this problem is standard, work in that direction suggested the process would be tedious, and the end result not particularly enlightening. Rather than pursuing it, we will focus on the numerical results for this case.

6. Numerical simulations of 2D katabatic flow (strip flow)

To confirm and extend the main results of the linear analysis of section 5, the numerical model outlined in section 4 was applied to laminar 2D katabatic flow induced by an isolated strip of constant negative surface buoyancy running down the slope. Several factors necessitated the use of a very broad (compared to the width of the strip) domain in the cross-slope direction. Firstly, in order to simulate an isolated strip in the presence of periodic-over-Y boundary conditions, very wide buffer zones of zero surface buoyancy were needed on either side of the strip. A series of preliminary experiments (not shown) suggested that for a strip of fixed cross-slope width l, increasing the size of the buffer zones led to proportional decreases in the cross-slope velocity and buoyancy at the top of the computational domain. This result was consistent with the analysis of the doubly-periodic case (1) in section 3: for a large but necessarily finite computational domain width $2L_y$, the $X-Y$ average surface buoyancy is not exactly zero, and so the buoyancy and cross-slope velocity far above the slope should not be exactly zero, but the values of those variables can be made arbitrarily small by making $2L_y$ sufficiently large. For the parameter values chosen in our experiments, buffer zones ten times the width of the strip resulted in values of buoyancy and cross-slope velocity at the top of the computational domain that were less than 10% of their peak values in the boundary layer. Secondly, in order to simulate a boundary-layer-like flow (subject of the linear analysis), it was necessary for the strip width to be much larger than the boundary-layer thickness. Finally, it was necessary to have enough grid points in the slope-normal direction to resolve flow features with strong vertical variations. The challenge was therefore to have enough grid points in the cross-slope direction that the inequalities $\Delta Z = \Delta Y \ll |M|^{-1}l_s \ll l \ll 2L_y$ were satisfied, where the Δ symbols denote the spacing in the corresponding direction. Our computational resources were insufficient to simulate the small-K flows discussed in subsection 5.2, but were marginally sufficient to satisfy the inequalities for some large-K flows analysed in subsection 5.3. Thus, we will focus here on large-K flows.

Experiments were conducted with Bu = 1, Re = 4.37 and $\alpha = 3°$ (so $K_{ref} \cong 0.088$). Each simulation was run until a steady state was attained. Of the simulated variables, the buoyancy field consistently had the simplest structure. It was dominated in the steady state by a nearly symmetric (with respect to centre of strip) boundary layer of negatively buoyant air capped by a shallow zone of positively buoyant air. The presence of this buoyancy maximum was robust in our experiments, and its elevation above the centre of the strip provided a convenient measure of boundary layer thickness z_{max}. Figure 6 depicts this boundary-layer thickness as a function of strip width. If the dominant K was proportional to the reciprocal non-dimensional strip width (although it is not clear what the constant of proportionality should be in
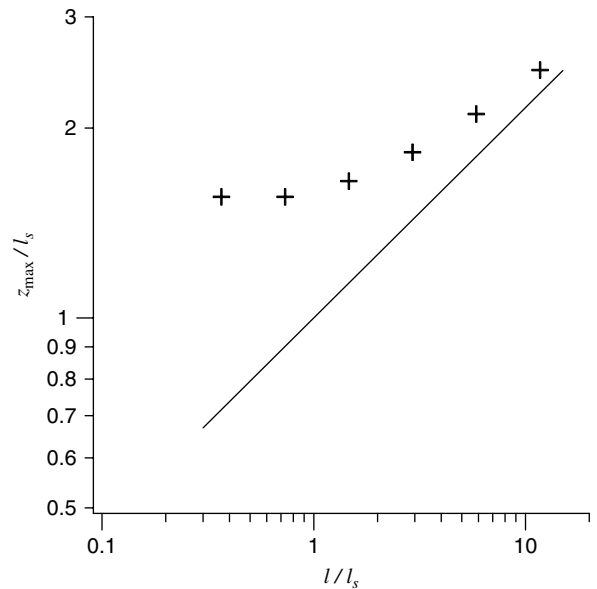

Figure 6. Steady-state boundary-layer thickness, estimated from the height of buoyancy maximum, as a function of strip width l in the katabatic flow with y heterogeneity described in the text. Symbols denote numerical data. Solid line depicts a theoretical 1/3 law for large-K flows.

that case, and the value of that constant could affect whether the large-K condition $K \gg K_{ref}$ was satisfied), then according to the linear theory, the boundary-layer thickness should grow as the 1/3 power of the strip width. According to Figure 6, the simulations with broader strips did exhibit an approximate 1/3 power law behaviour. That the flows with the smaller strip widths did not display this behaviour is not surprising since the boundary-layer concept on which the linear theory was based breaks down when the strip width and z_{max} are of similar magnitude (it can readily be inferred from Figure 6 that l is close to z_{max} when $l/l_s = 1$).

The flow variables in the steady state for the case where $l/l_s = 11.7$ are presented in Figure 7. Since the bulk of the computational domain was occupied by the buffer zones or by the region above the boundary layer, flow visualization was facilitated by only displaying variables in the lower half of the computational domain and in the vicinity of the negatively buoyant strip. The buoyancy field, the most symmetric of the variables, indicates a cold pool just above the negatively buoyant strip, capped by a small zone of positively buoyant air. The tendency of the cold air to spread laterally outward across the slope on either side of the strip (as in a density current) in a very shallow layer (approximately $z < 0.02$ km) is evident in the v field just above the strip. Above that thin layer of outflow is a much thicker zone of convergent flow ($\partial v/\partial y < 0$) and associated weak subsidence necessitated by mass conservation. The cold pool and the warm cap above it are located in this subsidence zone; the cold pool is forced by the surface buoyancy condition while the warm cap arises from subsidence in the stably-stratified environment. The velocity vectors in the $Y-Z$ cross-slope plane (Figure 8;
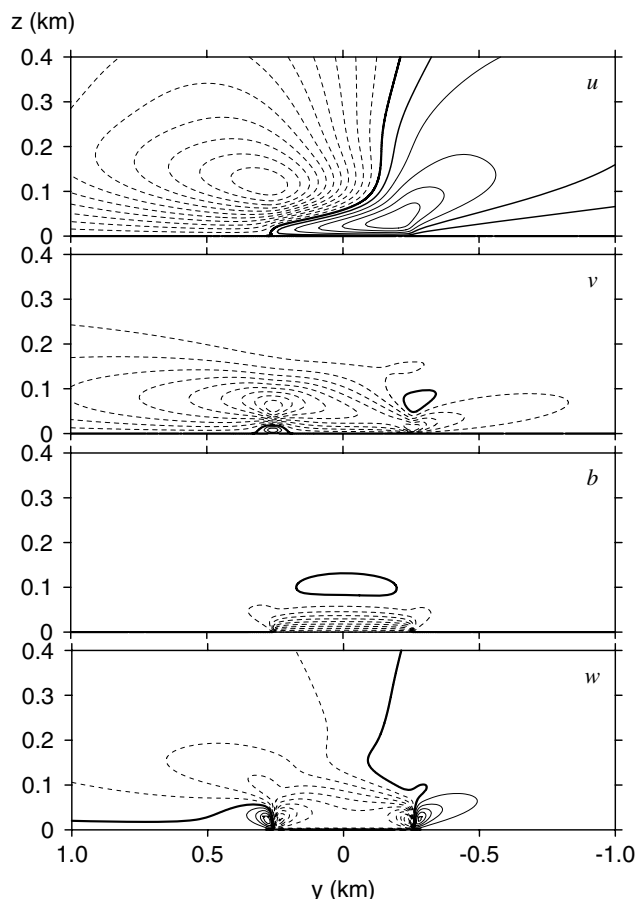
Figure 7. Contour plots of flow fields in the steady state for the 2D experiment with Re = 4.37, Bu = 1, and l/l_s = 11.7. The x axis is directed into the plot. Only the portion of the computational domain in the vicinity of the strip is shown. Contour intervals for u, v, b, and w are $2 \cdot 10^{-4}$ m s^{-1}, $2 \cdot 10^{-4}$ m s^{-1}, 10^{-3} m s^{-2}, and $5 \cdot 10^{-5}$ m s^{-1}, respectively. Negative contours are dashed. Zero contours are marked with bold solid lines.

further zoomed in to the immediate vicinity of the strip) indicate counter-rotating circulations on either side of the strip centred on baroclinic zones of strong cross-slope surface buoyancy gradient, a broad region of descent between the two circulation centres, and a pronounced cross-slope flow (from left to right) throughout the lower part of the domain. The left-to-right bias in the cross-slope flow just above the strip is due to the rightward

deflection of the primary katabatic downslope flow by the Coriolis force. Returning to Figure 7, we see that there is the expected downslope katabatic jet adjacent to the strip, but there is also substantial asymmetry in that flow component, with marked upslope flow throughout approximately the left half of the flow domain and downslope flow through the right half of the domain. Associated with this flow asymmetry is a broad area of positive slope-normal vorticity $\zeta = -\partial u/\partial y > 0$ over the strip. This slope-normal vorticity originates in the stretching term in the slope-normal vorticity equation: in the presence of cross-slope convergence ($-\partial v/\partial y > 0$), positive ζ is produced by the stretching of planetary vorticity, $-f\partial v/\partial y = f\partial w/\partial z > 0$. As seen in Figure 7, a broad zone of peak cross-slope convergence $-\partial v/\partial y$ at $z \approx 0.1$ km is closely associated with the broad zone of peak ζ ($= -\partial u/\partial y$).

Figure 7 also shows that U and W do not vanish at the half-way point to the top of the computational domain (top of the figures); neither do these fields vanish at the top of the computational domain. However, by checking points at the top of the computational domain, we verified that $-U\sin\alpha$ nearly cancelled with $W\cos\alpha$, indicating that the flow far above the slope was purely horizontal, as predicted by the linear theory.

In view of the flow structure described above, we can crudely infer the trajectories of air parcels in the regions well above the cold pool (say, $z > 0.2$ km) and in the lower part of the boundary layer.

In the upper region, a horseshoe-like circulation is found in which

(u.1) air parcels in the environment on the left of the strip (with respect to an observer looking downslope) enter the top of the sloping boundary layer horizontally along environmental isentropes, in a combined upslope $u < 0$ and toward-slope $w < 0$ flow, then

(u.2) move across the slope ($v < 0$) to the right side of the strip where u and w reverse sign, and then

(u.3) leave the boundary layer horizontally, along environmental isentropes.

The air circulation in the lower part of the boundary layer is more complicated. Most air parcels in this region
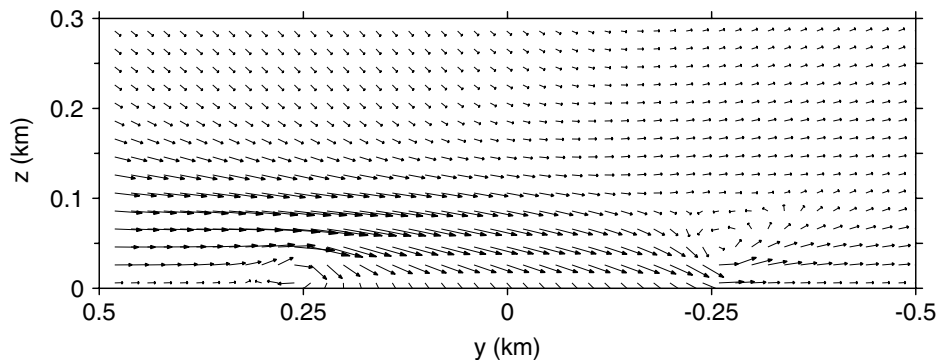

Figure 8. Velocity vectors in the y–z plane for the same experiment as in Figure 7. Vectors are displayed at every fifth grid point.
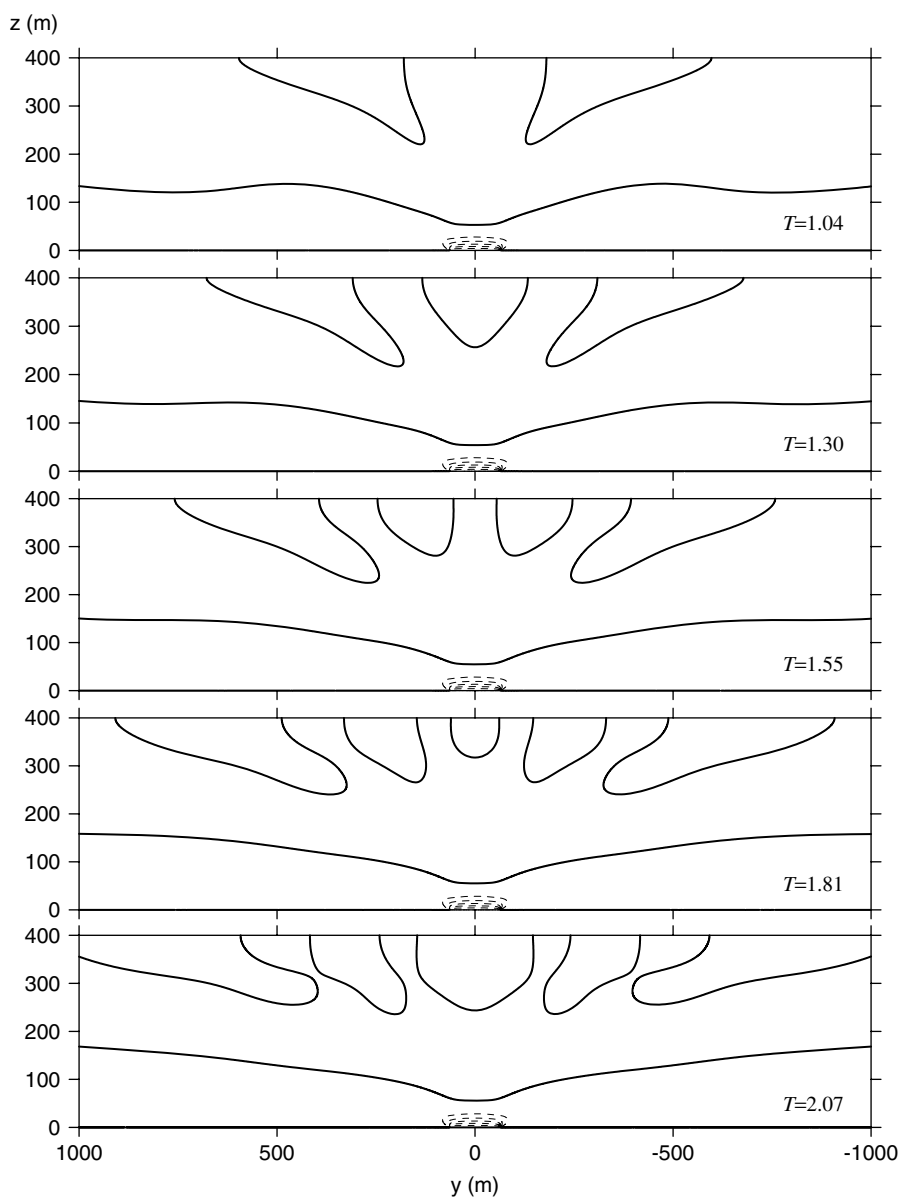
Figure 9. Contour plots of b in the y–z plane at five different times early in the simulation for the 2D experiment with Re $= 300$, Bu $= 1$, and $l/l_s = 1.28$. Negative contours are dashed. Zero contours are marked with bold solid lines.

(l.1) enter the boundary layer laterally, from the left side of the strip, and continue to move right while they also

(l.2) first move upslope ($u < 0$) and then downslope ($u > 0$), and then

(l.3) leave the boundary layer laterally on the right side of the strip.

However, other parcels at low altitudes exhibit more corkscrew-like trajectories, moving either up- or downslope as they get caught in the baroclinic circulations on either side of the strip.

Finally, we note that a common transient feature of all simulated flows was the generation and propagation of internal gravity waves. The waves were especially pronounced in the w and b fields in an experiment with a larger Reynolds number. The b field from an experiment with $l/l_s = 1.28$, Bu $= 1$, Re $= 300$ is presented at several early times in Figure 9. By tracking the position of the zero contours near the top of the figure we see that the waves originate over the centre of the strip and propagate toward the right and left across the slope. Observational studies have revealed the existence of low-frequency oscillatory disturbances superimposed on the mean katabatic flow (Tyson, 1968; Doran and Horst, 1981; Gryning *et al.*, 1985; Stone and Hoard, 1989; Helmis and Papadopoulos, 1996; Monti *et al.*, 2002). Several of these studies suggest that these oscillations are internal gravity waves.

7. Conclusions

Previous studies have shown that steady boundary-layer-type solutions for the buoyancy and cross-slope velocity

are unattainable when the classical 1D Prandtl framework of laminar katabatic flow along a uniformly cooled sloping surface (without linear radiative damping) is extended to include the Coriolis force. In the laminar case, the downslope velocity exhibits a boundary-layer structure, but the buoyancy and cross-slope velocity fields spread inexorably upward. To see if this non-intuitive behaviour was an artefact of the laminar flow constraint, we conducted direct numerical simulation (DNS) of turbulent katabatic flows with and without the Coriolis force. Since the turbulence was explicitly simulated in these DNS runs, there was no need for closure assumptions concerning the values of the eddy viscosity and diffusivity coefficients. However, it should be borne in mind that our turbulence simulations were carried out with a Reynolds number much smaller than those found in real katabatic flows. Our results suggest that, as in the laminar case, steady boundary-layer-like solutions for the buoyancy and cross-slope velocity variables are unattainable in the companion turbulent flow when the Coriolis force is included: there is an inexorable upward growth of the buoyancy and cross-slope velocity fields. Simulations with larger Reynolds numbers will be undertaken in the future, as computational resources permit.

Based on the analyses of Coriolis effects in katabatic flows in the atmosphere and related slope flows in the ocean, we suggest that processes that might be considered to be of secondary importance may, if persistent, prove to be vital in controlling the structure of the steady state, especially for the cross-slope velocity and buoyancy fields. In particular, provision for the finite nature of real surface forcings and slopes, which was not required to obtain steady boundary-layer-type buoyancy fields in the classical non-rotating theory, may be essential when provision is made for the Coriolis force. Linear theory and corresponding numerical simulations of rotating 2D flows forced by a cold strip of finite cross-slope extent running down the slope did predict a steady state in which the buoyancy and cross-slope velocity decayed far above the slope. On the other hand, the downslope and slope-normal velocity components did not vanish far above the slope. Rather, these components comprised two purely horizontal along-isentrope counter-flowing currents that intersected the sloping boundary layer: an upslope current entering the top of the boundary layer from the environment on one side of the strip, and a downslope current flowing out of the boundary layer into the environment on the other side of the strip. A vorticity-dynamics perspective reveals the pathway for the generation of these counter-flowing horizontal currents. Baroclinically generated counter-rotating circulations arising from the lateral finiteness of the strip (2D effects) produce a broad region of subsidence above the strip, with a layer of convergent cross-slope flow overlying a very shallow layer of divergent cross-slope flow adjacent to the slope. In the broad region of flow convergence, positive slope-normal vorticity is generated through the stretching of planetary vorticity. In this scenario, the slope-normal vorticity is manifested as a shear flow, two counter-flowing horizontal currents. The generation of this shear flow is thus analogous to the spin-up of a vortex over axisymmetric terrain (James, 1989; Parish and Bromwich, 1991; Parish, 1992), although in the latter case the subsidence and associated stretching of planetary vorticity arise from the primary katabatic flow down a conical slope, not from a secondary baroclinically-generated circulation associated with the finite cross-slope width of a strip.

In the future, we hope to explore the $Bu-Re-l/l_s$ parameter space for the strip problem in more detail, with special emphasis on flows with larger Re and l/l_s, as computational resources permit. We also plan to extend our 2D $(X-Z)$ similarity model of katabatic flow with downslope inhomogeneity (Shapiro and Fedorovich, 2007) to include the Coriolis force.

Acknowledgements

Appendix A. Generalizing (2.2) for Height-Dependent Eddy Viscosity and Diffusivity Coefficients

Equation (2.2) can be extended to a framework with height-dependent eddy viscosity and diffusivity coefficients through a very slight modification of the procedure outlined in section 2. We consider height variations of ν and κ that are quite general, the only restrictions being that the height dependences are the same (turbulent Prandtl number $Pr = \nu/\kappa$ is constant), and neither ν nor κ vanish at finite z. The extended 1D steady-state versions of (1.1)–(1.3) become

$$0 = N^2 u \sin\alpha + \frac{\mathrm{d}}{\mathrm{d}z}\left(\kappa(z)\frac{\mathrm{d}b}{\mathrm{d}z}\right), \qquad (A1)$$

$$0 = fv - b\sin\alpha + \frac{\mathrm{d}}{\mathrm{d}z}\left(\nu(z)\frac{\mathrm{d}u}{\mathrm{d}z}\right), \qquad (A2)$$

$$0 = -fu + \frac{\mathrm{d}}{\mathrm{d}z}\left(\nu(z)\frac{\mathrm{d}v}{\mathrm{d}z}\right). \qquad (A3)$$

Eliminating u between (A1) and (A3) yields,

$$N^2 \sin\alpha \frac{\mathrm{d}}{\mathrm{d}z}\left(\nu(z)\frac{\mathrm{d}v}{\mathrm{d}z}\right) + f\frac{\mathrm{d}}{\mathrm{d}z}\left(\kappa(z)\frac{\mathrm{d}b}{\mathrm{d}z}\right) = 0. \quad (A4)$$

Integrating (A4) and imposing (as before) the remote conditions $\mathrm{d}v/\mathrm{d}z$, $\mathrm{d}b/\mathrm{d}z \to 0$ as $z \to \infty$, we obtain

$$N^2 \sin\alpha \, \nu(z)\frac{\mathrm{d}v}{\mathrm{d}z} + f\kappa(z)\frac{\mathrm{d}b}{\mathrm{d}z} = 0. \qquad (A5)$$

Dividing (A5) by κ yields $N^2 \mathrm{Pr} \sin\alpha \, \mathrm{d}v/\mathrm{d}z + f \mathrm{d}b/\mathrm{d}z = 0$. Integrating this latter expression and imposing slope conditions of no-slip and specified buoyancy b_0, we obtain $N^2 \mathrm{Pr} \sin\alpha v + f b = f b_0$. Evaluating this result together with (A2) as $z \to \infty$ yields the remote ($z \to \infty$) values of b and v as

$$b_\infty = \frac{b_0}{1 + \mathrm{PrBu}}, \quad v_\infty = \frac{\sin\alpha \, b_0}{f(1 + \mathrm{PrBu})}, \quad \text{(A6)}$$

which is identical to (2.2). Thus, the remote values of b and v in the steady state are independent of the mixing coefficients (constant or height-dependent). The result is somewhat reminiscent of unsteady Couette flow (one rigid boundary moved suddenly and one end held stationary; p.190 of Batchelor, 1967). In that case the steady-state structure (terminal state of the unsteady problem) is independent of viscosity; viscosity only affects the time-scale for the attainment of the steady state.

Appendix B. Analytical Solution of (5.17)

In terms of a new variable $P \equiv M^2$, (5.17) becomes a cubic equation,

$$P^3 + \left(1 + \frac{1}{\mathrm{Bu}}\right)P - K^2\cot^2\alpha = 0, \quad M = \pm\sqrt{P}, \quad \text{(B1)}$$

which has the three roots (Abramowitz and Stegun, 1964, p. 17),

$$P_1 = s_1 + s_2, \quad P_2 = -\frac{1}{2}(s_1 + s_2) + \frac{\mathrm{i}\sqrt{3}}{2}(s_1 - s_2),$$

$$P_3 = -\frac{1}{2}(s_1 + s_2) - \frac{\mathrm{i}\sqrt{3}}{2}(s_1 - s_2), \quad \text{(B2)}$$

where

$$s_1 \equiv q^{1/2}\left\{\frac{r}{q^{3/2}} + \left(1 + \frac{r^2}{q^3}\right)^{1/2}\right\}^{1/3},$$

$$s_2 \equiv q^{1/2}\left\{\frac{r}{q^{3/2}} - \left(1 + \frac{r^2}{q^3}\right)^{1/2}\right\}^{1/3}, \quad \text{(B3)}$$

$$q \equiv \frac{1 + 1/Bu}{3}, \quad r \equiv \frac{K^2\cot^2\alpha}{2}. \quad \text{(B4)}$$

It is convenient to introduce a parameter ε defined as

$$\varepsilon \equiv \frac{r}{q^{3/2}} = \frac{3^{3/2}}{2}\frac{K^2\cot^2\alpha}{(1 + 1/Bu)^{3/2}}, \quad \text{(B5)}$$

in terms of which s_1 and s_2 become

$$s_1 = q^{1/2}\left\{(1 + \varepsilon^2)^{1/2} + \varepsilon\right\}^{1/3},$$

$$s_2 = -q^{1/2}\left\{(1 + \varepsilon^2)^{1/2} - \varepsilon\right\}^{1/3}. \quad \text{(B6)}$$

Since r and q (and hence ε) are real and positive, s_1 is real and positive, while s_2 is real and negative. Accordingly, P_3 and P_2 are complex conjugates of each other. We also note that since s_2 is negative and has a magnitude less than that of s_1 (which is positive), $s_1 + s_2$ is positive.

It is convenient to rewrite P_2 and P_3 in polar form. For P_2 we write $P_2 = \Phi_2 \exp(\mathrm{i}\lambda_2)$ where

$$\Phi_2 = q^{1/2}\left[\left\{(1 + \varepsilon^2)^{1/2} + \varepsilon\right\}^{2/3} + \left\{(1 + \varepsilon^2)^{1/2} - \varepsilon\right\}^{2/3} + 1\right]^{1/2}, \quad \text{(B7)}$$

$$\lambda_2 = \pi - \tan^{-1}\left(\sqrt{3}\left[\frac{\{(1+\varepsilon^2)^{1/2} + \varepsilon\}^{1/3} + \{(1+\varepsilon^2)^{1/2} - \varepsilon\}^{1/3}}{\{(1+\varepsilon^2)^{1/2} + \varepsilon\}^{1/3} - \{(1+\varepsilon^2)^{1/2} - \varepsilon\}^{1/3}}\right]\right), \quad \text{(B8)}$$

and the principal value of the inverse tangent function is taken. In arriving at (B8), we recognized that $\cos\lambda_2 < 0$ and $\sin\lambda_2 > 0$, and so identified λ_2 in the second quadrant.

Taking the square roots of these P, and rejecting the roots with positive real part to avoid growing solutions far above the slope, we obtain three physically acceptable roots M:

$$M_1 = -\left(\frac{1 + 1/\mathrm{Bu}}{3}\right)^{1/4}\left[\{(1+\varepsilon^2)^{1/2} + \varepsilon\}^{1/3} - \{(1+\varepsilon^2)^{1/2} - \varepsilon\}^{1/3}\right]^{1/2}, \quad \text{(B9)}$$

$$M_2 = -\left(\frac{1 + 1/\mathrm{Bu}}{3}\right)^{1/4}\left[\{(1+\varepsilon^2)^{1/2} + \varepsilon\}^{2/3} + \{(1+\varepsilon^2)^{1/2} - \varepsilon\}^{2/3} + 1\right]^{1/4}\mathrm{e}^{\mathrm{i}\lambda_2/2}, \quad \text{(B10)}$$

$$M_3 = M_2^*, \quad \text{(B11)}$$

where an asterisk (*) denotes complex conjugation. In arriving at the leading minus sign in (B10), we noted that since λ_2 is in the second quadrant, $\lambda_2/2$ is in the first quadrant, and so $\mathrm{e}^{\mathrm{i}\lambda_2/2}$ has positive real part.

References

Abramowitz M, Stegun IA. 1964. *Handbook of mathematical functions with formulas, graphs, and mathematical tables*. National Bureau of Standards Applied Mathematics Series No.55, US Dept. of Commerce: Washington D.C.

Atkinson BW. 1981. *Meso-scale atmospheric circulations*. Academic Press: New York.

Batchelor GK. 1967. *An introduction to fluid dynamics*. Cambridge University Press.

Brazel AJ, Fernando HJS, Hunt JCR, Selover N, Hedquist BC, Pardyjak E. 2005. Evening transition observations in Phoenix, Arizona. *J. Appl. Meteorol.* **44**: 99–112.

Defant F. 1949. Zur Theorie der Hangwinde, nebst Bemerkungen zur Theorie der Berg- und Talwinde. *Arch. Meteorol. Geophys. Bioklim. A* **1**: 421–450.

Doran JC, Horst TW. 1981. Velocity and temperature oscillations in drainage winds. *J. Appl. Meteorol.* **20**: 361–364.

Egger J. 1981. On the linear two-dimensional theory of thermally induced slope winds. *Beitr. Phys. Atmos.* **54**: 465–481.

Egger J. 1985. Slope winds and the axisymmetric circulation over Antarctica. *J. Atmos. Sci.* **42**: 1859–1867.

Egger J. 1990. 'Thermally forced flows: Theory.' Pp. 43–58 in *Atmospheric processes over complex terrain*, Blumen W (ed). Amer. Meteorol. Soc.: Boston, Massachusetts.

Fedorovich E, Nieuwstadt FTM, Kaiser R. 2001. Numerical and laboratory study of a horizontally evolving convective boundary layer. Part I: Transition regimes and development of the mixed layer. *J. Atmos. Sci.* **58**: 70–86.

Fernando HJS, Lee SM, Anderson J, Princevac M, Pardyjak E, Grossman-Clarke S. 2001. Urban fluid mechanics: Air circulation and contaminant dispersion in cities. *Environ. Fluid Mech.* **1**: 107–164.

Gallée H, Schayes G. 1994. Development of a three-dimensional meso-γ primitive equation model: Katabatic winds simulation in the area of Terra Nova Bay, Antarctica. *Mon. Weather Rev.* **122**: 671–685.

Garrett C. 1991. Marginal mixing theories. *Atmos.-Ocean* **29**: 313–339.

Garrett C, MacCready P, Rhines P. 1993. Boundary mixing and arrested Ekman layers: Rotating stratified flow near a sloping boundary. *Ann. Rev. Fluid Mech.* **25**: 291–323.

Grisogono B, Oerlemans J. 2001. Katabatic flow: Analytic solution for gradually varying eddy diffusivities. *J. Atmos. Sci.* **58**: 3349–3354.

Grisogono B, Oerlemans J. 2002. Justifying the WKB approximation in pure katabatic flows. *Tellus A* **54**: 453–462.

Gryning S-E, Mahrt L, Larsen S. 1985. Oscillating nocturnal slope flow in a coastal valley. *Tellus A* **37**: 196–203.

Gutman LN. 1983. On the theory of the katabatic slope wind. *Tellus A* **35**: 213–218.

Gutman LN, Malbakhov VM. 1964. On the theory of katabatic winds of Antarctic. *Meteorol. Issled.*, **9**: (in Russian) 150–155.

Gutman LN, Melgarejo JW. 1981. On the laws of geostrophic drag and heat transfer over a slightly inclined terrain. *J. Atmos. Sci.* **38**: 1714–1724.

Helmis CG, Papadopoulos KH. 1996. Some aspects of the variation with time of katabatic flow over a simple slope. *Q. J. R. Meteorol. Soc.* **122**: 595–610.

Hunt JCR, Fernando HJS, Princevac M. 2003. Unsteady thermally driven flows on gentle slopes. *J. Atmos. Sci.* **60**: 2169–2182.

Ingel' LKh. 2000. Nonlinear theory of slope flows. *Atmos. Oceanic Phys. (Izvestiya)* **36**: 384–389.

James IN. 1989. The Antarctic drainage flow: Implications for hemispheric flow on the Southern Hemisphere. *Antarct. Sci.* **1**: 279–290.

Kavčič I, Grisogono B. 2007. Katabatic flow with Coriolis effect and gradually varying eddy diffusivity. *Boundary-Layer Meteorol.* **125**: 377–387.

Kondo H. 1984. The difference of the slope wind between day and night. *J. Meteorol. Soc. Jpn* **62**: 224–233.

Lee S-M, Fernando HJS, Princevac M, Zajic D, Sinesi M, McCulley JL, Anderson J. 2003. Transport and diffusion of ozone in the nocturnal and morning planetary boundary layer of the Phoenix valley. *Environ. Fluid Mech.* **3**: 331–362.

Lu R, Turco RP. 1994. Air pollutant transport in a coastal environment. Part I: Two-dimensional simulations of sea-breeze and mountain effects. *J. Atmos. Sci.* **51**: 2285–2308.

Lykosov VN, Gutman LN. 1972. Turbulent boundary layer above a sloping underlying surface. *Atmos. Ocean. Phys. (Izvestiya)* **8**: 799–809.

MacCready P, Rhines PB. 1991. Buoyant inhibition of Ekman transport on a slope and its effect on stratified spin-up. *J. Fluid Mech.* **223**: 631–661.

MacCready P, Rhines PB. 1993. Slippery bottom boundary layers on a slope. *J. Phys. Oceanogr.* **23**: 5–22.

Mahrt L. 1982. Momentum balance of gravity flows. *J. Atmos. Sci.* **39**: 2701–2711.

Monti P, Fernando HJS, Princevac M, Chan WC, Kowalewski TA, Pardyjak ER. 2002. Observations of flow and turbulence in the nocturnal boundary layer over a slope. *J. Atmos. Sci.* **59**: 2513–2534.

Nieuwstadt FTM. 1990. 'Direct and large-eddy simulation of free convection.' Pp. 37–47 in *Proc. 9th International Heat Transfer Conference*, 19–24 August 1990, Jerusalem, Israel. Amer. Soc. Mech. Eng.: New York.

Oerlemans J. 1998. 'The atmospheric boundary layer over melting glaciers.' Pp. 129–153 in *Clear and cloudy boundary layers*, Holtslag AAM, Duynkerke PG (eds). Royal Netherlands Academy of Arts and Sciences.

Papadopoulos KH, Helmis CG, Soilemes AT, Kalogiros J, Papageorgas PG, Asimakopoulos DN. 1997. The structure of katabatic flows down a simple slope. *Q. J. R. Meteorol. Soc.* **123**: 1581–1601.

Parish TR. 1992. On the role of Antarctic katabatic winds in forcing large-scale tropospheric motions. *J. Atmos. Sci.* **49**: 1374–1385.

Parish TR, Bromwich DH. 1991. Continental-scale simulation of the Antarctic katabatic wind regime. *J. Climate* **4**: 135–146.

Parish TR, Waight KT. 1987. The forcing of Antarctic katabatic winds. *Mon. Weather Rev.* **115**: 2214–2226.

Prandtl L. 1942. *Führer durch die Strömungslehre*. Vieweg und Sohn: Braunschweig.

Renfrew IA. 2004. The dynamics of idealized katabatic flow over a moderate slope and ice shelf. *Q. J. R. Meteorol. Soc.* **130**: 1023–1045.

Renfrew IA, Anderson PS. 2006. Profiles of katabatic flow in summer and winter over Coats Land, Antarctica. *Q. J. R. Meteorol. Soc.* **132**: 779–802.

Shapiro A, Fedorovich E. 2004. Prandtl number dependence of unsteady natural convection along a vertical plate in a stably stratified fluid. *Int. J. Heat and Mass Transfer* **47**: 4911–4927.

Shapiro A, Fedorovich E. 2006. Natural convection in a stably stratified fluid along vertical plates and cylinders with temporally periodic surface temperature variations. *J. Fluid Mech.* **546**: 295–311.

Shapiro A, Fedorovich E. 2007. Katabatic flow along a differentially cooled sloping surface. *J. Fluid Mech.* **571**: 149–175.

Stiperski I, Kavčič I, Grisogono B, Durran DR. 2007. Including Coriolis effects in the Prandtl model for katabatic flow. *Q. J. R. Meteorol. Soc.* **133**: 101–106.

Stone GL, Hoard DE. 1989. Low-frequency velocity and temperature fluctuations in katabatic valley flows. *J. Appl. Meteorol.* **28**: 477–488.

Thorpe SA. 1987. Current and temperature variability on the continental slope. *Philos. Trans. R. Soc. London A* **323**: 471–517.

Tyson PD. 1968. Velocity fluctuations in the mountain wind. *J. Atmos. Sci.* **25**: 381–384.

Whiteman CD. 1990. 'Observations of thermally developed wind systems in mountainous terrain.' Pp. 5–42 in *Atmospheric processes over complex terrain*, Blumen W (ed). Amer. Meteorol. Soc.: Boston, Massachusetts.

Whiteman CD. 2000. *Mountain meteorology: Fundamentals and applications*. Oxford University Press.

Copyright © 2008 Royal Meteorological Society

Q. J. R. Meteorol. Soc. **134**: 353–370 (2008)